Volume 5
Number 3
March 2025
Pages 263–408

Environmental Science
Atmospheres

rsc.li/esatmospheres

ISSN 2634-3606

ROYAL SOCIETY OF CHEMISTRY

PAPER

Bethany Sutherland and Nicholas Meskhidze
Assessment of high spectral resolution lidar-derived $PM_{2.5}$ concentration from SEAC^{4}RS, ACEPOL, and three DISCOVER-AQ campaigns

Environmental Science: Atmospheres

ROYAL SOCIETY OF CHEMISTRY

PAPER

View Article Online
View Journal | View Issue

Cite this: *Environ. Sci.: Atmos.*, 2025, **5**, 270

Assessment of high spectral resolution lidar-derived $PM_{2.5}$ concentration from SEAC^{4}RS, ACEPOL, and three DISCOVER-AQ campaigns†

Bethany Sutherland ‡ and Nicholas Meskhidze *

Received 29th October 2024
Accepted 11th February 2025

DOI: 10.1039/d4ea00143e

rsc.li/esatmospheres

$PM_{2.5}$ (particulate matter with an aerodynamic diameter of less than 2.5 μm) exposure at elevated levels has been associated with adverse health outcomes. However, the high spatiotemporal variability of aerosols poses challenges in monitoring $PM_{2.5}$ using ground-based measurement networks. Previously, we developed a new method (referred to as HSRL-CH) to estimate surface $PM_{2.5}$ concentration and chemical composition using High Spectral Resolution Lidar (HSRL)-retrieved extinction and derived aerosol types. In this study, we evaluate HSRL-CH performance across the United States using HSRL retrievals from five campaigns: DISCOVER-AQ California, SEAC^{4}RS, DISCOVER-AQ Texas, DISCOVER-AQ Colorado, and ACEPOL. We assess the remotely derived $PM_{2.5}$ estimates against measurements from the EPA Air Quality System (AQS) and compare HSRL-CH-derived aerosol chemical compositions with AQS-measured compositions. Across all campaigns, HSRL-CH-derived $PM_{2.5}$ shows a mean absolute error (MAE) of 10.2 μg m^{-3}. The DISCOVER-AQ California campaign had the highest MAE (14.8 μg m^{-3}), while other campaigns had MAE ≤ 7.2 μg m^{-3}. The lowest MAE occurs when dusty mix type aerosols dominate the retrieved aerosol optical depth, while the highest MAE is associated with smoke type aerosols. Different planetary boundary layer height estimates can lead to a 20% difference in MAE. We anticipate that the HSRL-CH method will provide reliable estimates of $PM_{2.5}$ concentration and chemical composition once satellite-based HSRL data acquisition becomes feasible.

Environmental significance

Our study introduces an innovative approach for determining both $PM_{2.5}$ concentrations and their chemical composition using remotely sensed observations. The key innovation lies in our use of high spectral resolution lidar (HSRL) data. Having previously demonstrated success with DISCOVER-AQ Baltimore–Washington data in the United States and KORUS-AQ in South Korea, we now expand our validation to include HSRL measurements from five additional field campaigns: DISCOVER-AQ (California, Texas, and Colorado), SEAC^{4}RS, and ACEPOL. The findings pave the way for satellite-based HSRL applications, enhancing aerosol monitoring and public health insights.

1 Introduction

Particulate matter with an aerodynamic diameter of less than 2.5 μm ($PM_{2.5}$) has been linked to a variety of respiratory and cardiovascular problems.[1–5] The surface concentration of $PM_{2.5}$ has been designated as one of the criteria pollutants[6] and is monitored and regulated by the U.S. Environmental Protection Agency (EPA). Despite its importance, monitoring of $PM_{2.5}$ remains predominantly limited to highly populated areas or regions of known concern, leaving large portions of the population unrepresented.[7,8] To fill the gaps in ground measurements of $PM_{2.5}$, much work has been done to remotely monitor the amount of particulate matter in the air and estimate the concentration of aerosols at the surface (*e.g.* ref. 7 and 9–12).

Despite advancements in remote sensing techniques, accurately estimating surface $PM_{2.5}$ concentrations remains a complex challenge due to several factors. In addition to microphysical properties such as size and shape, the optical properties of aerosols depend on their chemical composition.[13–16] For example, aerosols predominantly composed of black carbon exhibit much stronger radiation absorption in the visible range than aerosols composed primarily of sulfate, which mainly scatter radiation.[17] Additionally, the uptake of water by aerosol particles alters their optical properties.[14,18] However, this hygroscopic behavior is highly dependent on the specific composition of the aerosol.[19] Given these challenges, incorporating information about the

North Carolina State University, 2800 Faucette Drive Campus Box 8208, Raleigh, NC 27695, USA. E-mail: nmeskhidze@ncsu.edu

† Electronic supplementary information (ESI) available. See DOI: https://doi.org/10.1039/d4ea00143e

‡ Now at the Woodwell Climate Research Center, USA.

likely composition of aerosols becomes crucial for improving the accuracy of $PM_{2.5}$ estimates derived from remote sensing methods.

Meskhidze *et al.* developed an aerosol type-based remote sensing methodology, referred to as HSRL-CH, for estimating $PM_{2.5}$ concentrations.[20] This approach integrates airborne High Spectral Resolution Lidar (HSRL)-retrieved extinction data and derived aerosol types (*i.e.*, dusty mix, maritime, smoke, fresh smoke, and urban) with chemical composition information specific to each aerosol type. The chemical composition data are obtained through a combination of GEOS-Chem modeling and the Creating Aerosol Types from CHemisty (CATCH) algorithm.[21] A key strength of the HSRL-CH method lies in its ability to account for the varying hygroscopic properties and dry mass extinction coefficients of individual species (organics, black carbon, *etc.*). This is achieved by leveraging the intrinsic properties of aerosols as determined by their assigned type.

The HSRL-CH method has been tested using data from two campaigns with considerably different meteorological conditions and aerosol sources: the Deriving Information on Surface conditions from Column and Vertically Resolved Observations Relevant to Air Quality (DISCOVER-AQ) Baltimore–Washington D.C. campaign[20] and the Korea–United States Air Quality (KORUS-AQ) campaign.[22] When applied to retrievals from these campaigns, the agreement between surface $PM_{2.5}$ measurements and $PM_{2.5}$ estimated using the HSRL-CH method was comparable to or better than that of $PM_{2.5}$ simulated using state-of-the-art models such as GEOS-Chem and Community Multiscale Air Quality Modeling (CMAQ). The Mean Absolute Error (MAE) between the HSRL-CH methodology and AQS sites during the DISCOVER-AQ Baltimore–Washington D.C. campaign was 6.2 μg m^{-3}, while the CMAQ model showed an MAE of 9.2 μg m^{-3} (33% higher). During the KORUS-AQ campaign, the HSRL-CH methodology's MAE of 12.5 μg m^{-3} was 36% lower than that of CMAQ simulations (MAE = 19.4 μg m^{-3}) and 39% lower than that of GEOS-Chem simulations (20.5 μg m^{-3}) when compared to $PM_{2.5}$ measured at National Institute of Environmental Research (NIER) ground sites.

This study builds upon the work of Meskhidze *et al.*[20] and Sutherland *et al.*,[22] addressing a key limitation in their research: the insufficient validation of GEOS-Chem/CATCH-derived aerosol type-specific compositions due to limited collocated HSRL aerosol type retrievals and *in situ* composition measurements. We significantly expand the scope of analysis by incorporating data from five additional campaigns, encompassing nearly one hundred research flights with NASA HSRL retrievals across the United States. This expanded dataset offers a more comprehensive view across diverse geographic regions, seasons, and years, enabling a more rigorous testing of the HSRL-CH method and providing deeper insights into the chemical composition of each HSRL-derived aerosol type. Our analysis compares surface $PM_{2.5}$ estimates along flight tracks from three DISCOVER-AQ campaigns, the Aerosol Characterization from the Polarimeter and Lidar (ACEPOL) campaign, and the Studies of Emissions and Atmospheric Composition, Clouds and Climate Coupling by Regional Surveys (SEAC^{4}RS) campaign to measurements from EPA Air Quality System (AQS) sites. This extensive comparison enhances our understanding of the HSRL-CH method's performance across varied conditions and improves our ability to characterize aerosol compositions associated with different HSRL-derived types, ultimately advancing our capability to estimate $PM_{2.5}$ concentrations through remote sensing techniques.

2 Data

The data for the field campaigns are publicly available in the mission archives (see the Data availability section). The DISCOVER-AQ California (CA) campaign took place in January and February 2013 with flights predominantly conducted in the San Joaquin Valley. The DISCOVER-AQ Texas (TX) campaign took place in September 2013 with flights around the Houston area and the northern Gulf of Mexico. The DISCOVER-AQ Colorado (CO) campaign happened in July and August 2014 and consisted of flights mainly in the area between Denver and Cheyenne, Wyoming, but with a few flights extending east into neighboring states even as far as Virginia. The ACEPOL campaign took place in California and neighboring states during October and November of 2017. The SEAC^{4}RS campaign took place in August and September of 2013 with flights ranging from off the west coast of the U.S. to Georgia and from Canada to the Gulf of Mexico.

2.1 AQS measurements

This study compares remotely derived $PM_{2.5}$ with surface measurements collected at the EPA AQS sites. We utilize reported hourly averaged $PM_{2.5}$ data (parameter code 88101) from 23 AQS sites (ESI Table 1S†) located near one or more of the research flights.

Chemical speciation data are collected at select AQS sites every 3 or 6 days and averaged over 24 hours. The 99 flights conducted across the five campaigns resulted in 25 days where HSRL extinction retrievals and assigned aerosol types coincided with data collection at 10 different speciation sites (see Table 1). Concentrations for each species – sulfate + nitrate + ammonium (SNA), organic matter (OM), black carbon (BC), dust, and sea salt – in μg m^{-3} were calculated using the AQS parameter codes as described in Meskhidze *et al.*[20] ESI Table 2S† summarizes the

Table 1 List of AQS sites with speciation measurements used in this analysis

ID	AQS site ID	Location (latitude [°N], longitude [°E])
A	06_107_2002	Visalia, CA (36.332179, −119.291228)
B	06_019_0011	Fresno, CA (36.78538, −119.77321)
C	06_029_0014	Bakersfield, CA (35.356615, −119.062613)
D	06_059_0007	Anaheim, CA (33.83062, −117.93845)
E	06_099_0005	Modesto, CA (37.642165, −120.994212)
F	48_203_0002	Marshall, TX (32.669001, −94.167468)
G	48_201_1039	Deer Park, TX (29.670025, −95.128508)
H	08_031_0026	Denver, CO (39.77949, −105.00518)
I	08_001_0006	Commerce City, CO (39.826007, −104.937438)
J	08_123_0008	Platteville, CO (40.209387, −104.82405)

EPA parameter codes and derivation process for each aerosol species examined in this study.

2.2 HSRL-retrievals

The NASA LaRC second generation HSRL-2 [23,24] was flown on the NASA B200 aircraft during the DISCOVER-AQ CO, DISCOVER-AQ TX, and DISCOVER-AQ CA campaigns and on the ER-2 aircraft during ACEPOL. The DIAL-HSRL instrument[23,25] was flown on NASA's DC-8 aircraft during SEAC^{4}RS.

Burton *et al.* demonstrated that NASA HSRL retrievals could be used to classify aerosols into types such as ice, pure dust, dusty mix, maritime, polluted maritime, urban, fresh smoke, and smoke.[26] Types are classified based on the following aerosol intensive properties: aerosol depolarization (532 nm), aerosol lidar ratio (532 nm), aerosol backscatter color ratio (the ratio of aerosol backscatter coefficients at 532 nm and 1064 nm), and the spectral depolarization ratio (the ratio of depolarization ratios at 1064 nm and 532 nm). Both the HSRL-2 and the DIAL-HSRL perform the retrievals necessary to assign aerosol types using the methodology of Burton *et al.*[26] HSRL retrievals and assigned aerosol types were obtained from the campaign data archives. Instances of multiple consecutive retrievals being logged at the same time were corrected by assuming that each retrieval was 0.0028 hours after the previous one.

For comparison with surface measurements, we use HSRL retrievals within 8 km of the measurement location (see Section 3.3), following Meskhidze *et al.*[20] and Sutherland *et al.*[22] When comparing with AQS $PM_{2.5}$ data, we use HSRL retrievals from the same hour for hourly measurements and from the same day for daily speciation data.

2.3 Vertical mixing height

There is general consensus that the planetary boundary layer height (PBLH) and the mixing layer height (MLH) significantly influence surface air quality. The PBL is the portion of the troposphere directly influenced by surface properties (*e.g.* turbulence, convection, and sensible and latent heat flux), whereas the MLH describes the depth of turbulent mixing specifically.[27] Although PBLH and MLH are distinct concepts, both provide valuable insights into the atmospheric layer directly influenced by Earth's surface over short time periods.[28] However, neither PBLH nor MLH can be measured directly. Their values depend on both the calculation algorithms used and the instruments employed, leading to significant discrepancies in estimated values.[29–32] We utilize three different approaches to estimate this well-mixed layer: PBLH predicted by the North American Mesoscale Forecast System (NAM),[33] PBLH estimates from NASA's Modern-Era Retrospective Analysis for Research and Applications, version 2 (MERRA-2) reanalysis,[34] and MLH values derived from HSRL retrievals.[35,36] The use of multiple metrics allows for a more comprehensive understanding of the vertical structure of the atmosphere and helps to mitigate potential biases or limitations inherent in any single approach.

Previous studies[20,22] have shown that the application of HSRL retrievals for surface $PM_{2.5}$ predictions presents an additional challenge: extinction and aerosol types cannot be reported within ~300 m of the surface due to potential ground return interference with the atmospheric signal. To address this limitation, in previous studies we assumed that conditions above 300 m could represent surface conditions. While this assumption may hold true for well-mixed atmospheres with significant vertical extent, it may not be valid for shallow PBLH or MLH conditions, especially given significant model and measurement uncertainties.

2.4 Hygroscopic growth of particles

Relative humidity (RH)-dependent scattering enhancements caused by the water uptake of aerosols (hygroscopic growth) were calculated using species-specific hygroscopic growth factors following Meskhidze *et al.*[20] and Sutherland *et al.*[22] For organic matter, hygroscopic growth at 532 nm is calculated as $f_{OM} = 1 + 0.03 \times RH/(100 - RH)$ following ref. 14. Hygroscopic growth of sea salt is calculated as $f_{SS} = 1 + 21.13\left(\frac{RH}{100}\right)^{10.81}$ following ref. 37 for the fit at 550 nm. Hygroscopic growth for SNA is taken from Table 3 of ref. 15 for small sulfate and nitrate particles. The RH values were taken from the MERRA-2 reanalysis as in Sutherland *et al.*[22]

3. Methodology

3.1 HSRL data processing

The methodology for processing aerosol type and extinction data was largely based on the approaches described in Meskhidze *et al.*[20] and Sutherland *et al.*,[22] with some adjustments. We opted not to use the HSRL cumulative aerosol optical depth (Column_AOT_prfl) product to fill in gaps in the HSRL-retrieved extinctions, as this method produced noisy near-surface extinction results. Instead, we solely relied on the reported HSRL extinction at 532 nm (σ_{HSRL}). We modified the assumption about extending the lowest assigned aerosol types to the surface. In this study, we only applied this assumption when the lowest assigned types were within the NAM PBLH. Following Sutherland *et al.*,[22] we consolidated certain aerosol categories: the HSRL-assigned pure dust and dusty mix types were combined into a single "dusty mix" category and the polluted maritime and maritime types were combined into a single "maritime" category. These modifications aimed to improve the accuracy and consistency of the aerosol data processing while maintaining compatibility with previous studies.

3.2 Derived chemical components for different aerosol types

Aerosol chemical compositions for HSRL-retrieved aerosol types were derived using the CATCH algorithm[21] as discussed in Meskhidze *et al.*[20] and Sutherland *et al.*[22] CATCH was designed to assign aerosol types analogous to the HSRL-derived types based on GEOS-Chem modeled parameters as a means to link remotely sensed aerosol types with specific aerosol chemical composition. CATCH classifies aerosol type according to the Mahalanobis distance from a pre-specified cluster and was trained using HSRL derived aerosol types from the Ship-Aircraft

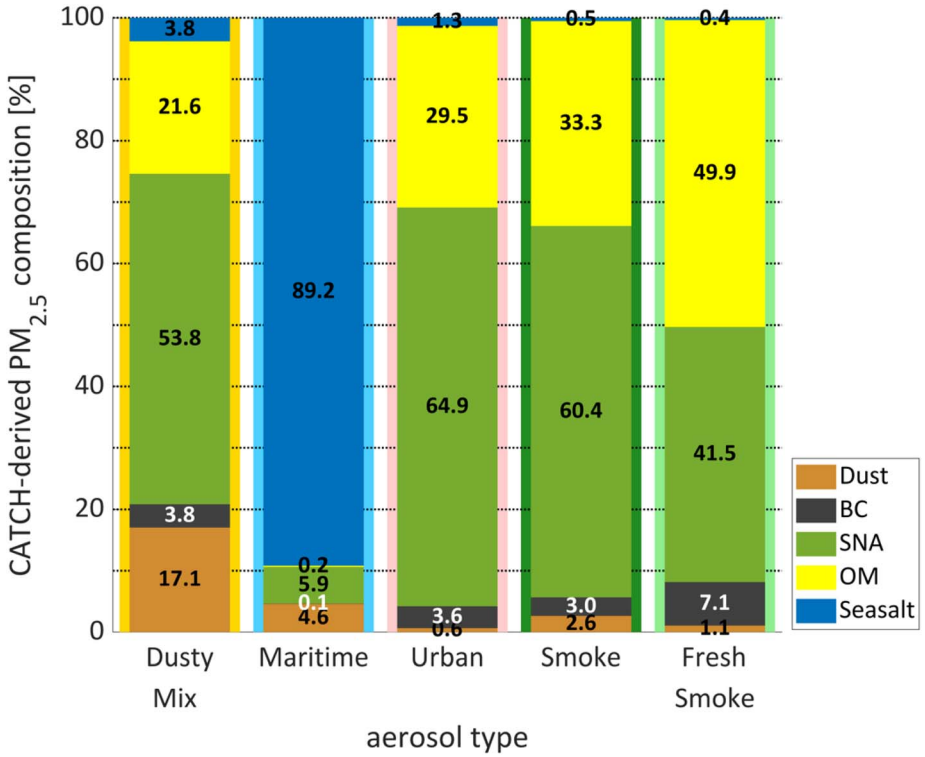

Fig. 1 CATCH-derived $PM_{2.5}$ chemical composition (the proportion of the mass of each aerosol type, which comprises dust, black carbon (BC), sulfate + nitrate + ammonium (SNA), organic matter (OM) and sea salt) for each aerosol type.

Bio-Optical Research (SABOR) campaign. However, for the dusty mix aerosol type, we diverged from the CATCH-derived composition and instead used prescribed mass fractions based on the findings of Shin *et al.*,[38] following the approach of Sutherland *et al.*[22] This adjustment was necessary because the CATCH-derived dust proportion was excessively high for accurately representing continental aerosols. It is worth noting that for all aerosol types, the majority of the mass is composed of hygroscopic species, underscoring the importance of composition information in properly accounting for hygroscopic growth. The normalized chemical composition (where the fractional contribution of all species totals 100%) for each aerosol type used in this study is presented in Fig. 1.

3.3 HSRL-CH method for $PM_{2.5}$ estimation

Meskhidze *et al.*[20] developed the HSRL-CH method for estimating atmospheric $PM_{2.5}$ and aerosol chemical makeup using the HSRL-retrieved aerosol extinction values and types. In this method, $PM_{2.5}$ is estimated as

$$[\mathrm{PM}_{2.5\ \mathrm{HSRL\text{-}CH}}] = \frac{\sigma_{\mathrm{HSRL}}}{\left(\sum_{j=1}^{5} b_j f_j(\mathrm{RH}) R_j\right)} \quad (1)$$

where j (=1, 2, … 5) refers to chemical species (SNA, OM, BC, dust, and sea salt). The relative abundance of each species is accounted for using $R_j = \sum_i \mathrm{type}_i K_{i,j}$, where type_i is the proportion of extinction within the grid that is assigned to aerosol type i (*i.e.*, dusty mix, maritime, urban, smoke, and fresh smoke), and $K_{i,j}$ is the mass fraction of species j for aerosol type i (as shown in Fig. 1 divided by 100%). As $PM_{2.5}$ is estimated on the HSRL retrieval grid, type_i can only be equal to 0 or 1. b_j and f_j(RH) are the dry mass extinction efficiencies and RH-dependent hygroscopic growth factors for each species as described in Section 2.4. We use dry mass extinction coefficients $b_{\mathrm{SNA}} = 3.0$, $b_{\mathrm{OM}} = 4.0$, $b_{\mathrm{BC}} = 10.0$, $b_{\mathrm{Dust}} = 1.0$, and $b_{\mathrm{Seasalt}} = 1.37$ $\mathrm{m^2\ g^{-1}}$.[15,39,40] As $PM_{2.5}$ is directly proportional to the retrieved extinction in eqn (1), relative errors in the retrieved extinction will correspond to proportional error in the derived $PM_{2.5}$. Rogers *et al.* performed a comparison of AOD and extinction retrievals from other contemporary instruments and the NASA Langley HSRL.[41]

HSRL retrievals of aerosol extinction are not reported within about 300 m of the surface, and the HSRL flight paths do not directly overpass the location of the AQS measurement sites. Therefore, the estimation of surface $PM_{2.5}$ involves an averaging process using the HSRL-CH method-derived $PM_{2.5}$ data. All data points are averaged below a specific mixing height vertically (see Section 4.1) and horizontally for all retrievals within an 8 km diameter circle centered on the AQS measurement stations. This 8 km colocation distance was determined to be appropriate for use with HSRL-CH in the Baltimore–Washington area, based on findings from Meskhidze *et al.*[20] To generate a continuous $PM_{2.5}$ profile along a flight path, the $PM_{2.5}$ value at each location is calculated by averaging all retrievals within an 8 km radius of that point. It is important to note that any retrievals lacking an assigned aerosol type are excluded from this analysis.

An important consideration is the impact of inexact colocation criteria when validating the remote sensing methodology using hourly $PM_{2.5}$ concentrations and daily averaged $PM_{2.5}$ compositions. As was noted in Dawson *et al.*, atmospheric conditions that create highly inhomogeneous aerosol distributions across space (8 km and within the PBLH) and time (hourly or daily) are inherently less suitable for comparison with surface measurements.[22] This limitation does not necessarily reflect the effectiveness of the HSRL-CH method but rather highlights the challenges of validation using data from field campaigns designed for different scientific objectives.

4 Results and discussion

4.1 Designation of vertical mixing height

The relationship between surface $PM_{2.5}$ and remotely retrieved aerosol optical depth (AOD) has been a subject of interest in various studies. Previous studies have shown that these two measurements can be poorly correlated when aerosol plumes are elevated above the boundary layer or the boundary layer is not well mixed.[9,42–44] Lidars can provide the vertical curtains of aerosol extinction, allowing for a more detailed understanding of aerosol distribution throughout the atmospheric column. When using the HSRL-CH methodology to estimate surface $PM_{2.5}$, concentrations, a critical consideration emerges: determining the appropriate vertical extent of retrievals that can accurately represent the surface conditions. The importance of this vertical extent selection stems from the need to capture the aerosol characteristics that are most representative of ground-level conditions while avoiding the inclusion of elevated plumes that may not influence surface air quality.

Fig. 2 presents a comparison of NAM PBLH, MERRA-2 PBLH, and HSRL-derived MLH for instances when the HSRL was within 8 km of an AQS site. The analysis revealed an average difference of 361 ± 541 m between these estimates. This substantial variability indicates that the choice of height parameter can significantly influence the vertical range of retrievals included when deriving surface $PM_{2.5}$ using the HSRL-CH methodology. For shallow PBLH or MLH conditions, it becomes difficult to determine whether the lowest HSRL retrievals originate from within the boundary layer or free troposphere, complicating accurate interpretation. Furthermore, when the estimated mixing height is lower, fewer vertical retrievals are available. This can amplify the influence of outliers (potentially related to local inhomogeneities), leading to significant effects on the derived surface $PM_{2.5}$ values. These findings underscore the critical importance of carefully selecting the vertical mixing height estimation method when applying the HSRL-CH methodology for surface $PM_{2.5}$ derivation.

Table 2 provides a summary of the statistical comparison between HSRL-CH-derived and AQS-measured $PM_{2.5}$. The table includes key metrics such as the mean absolute error (MAE), the normalized mean absolute error (NMAE), the mean error (ME), the coefficient of determination (r^2), and the number of data points (N). A notable finding from this comparison is that different choices for the vertical extent of retrievals can result in ~20% variability in the MAE, ME, and r^2 values. Despite this variability, the analysis does not conclusively demonstrate a clear advantage of one methodology over the others. Given this lack of definitive superiority, we have opted for simplicity in our approach for the remainder of this study. Specifically, we

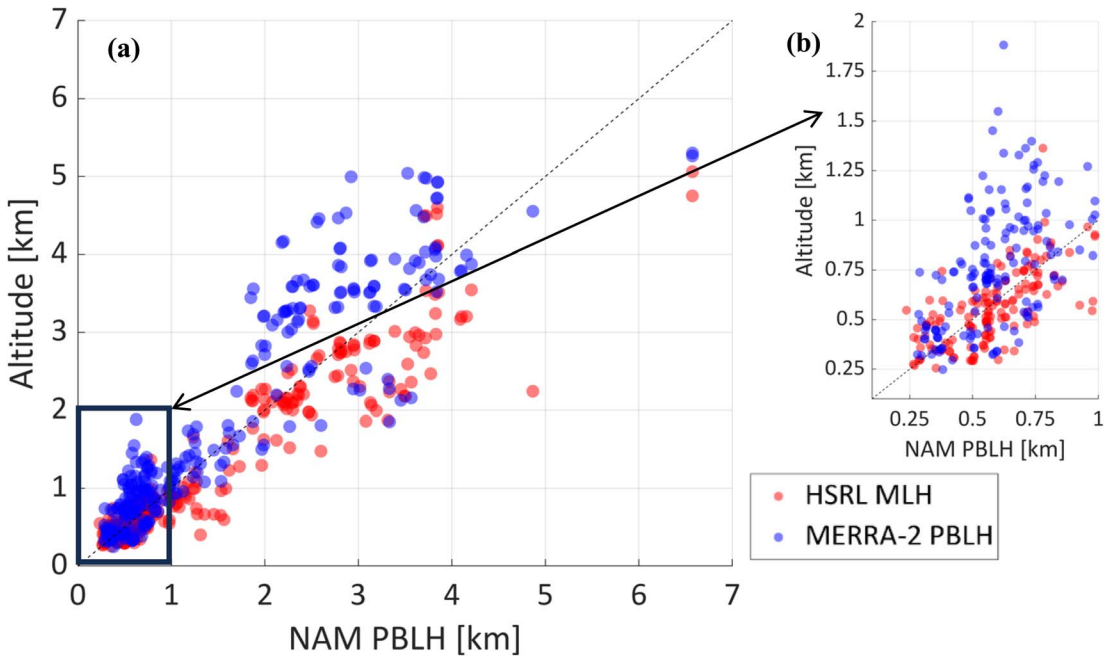

Fig. 2 (a) NAM PBLH *vs.* HSRL MLH (red markers) and MERRA-2 PBLH (blue markers) for all times when a flight path was within 8 km of one of the AQS sites, and (b) zoomed in to only show cases where NAM PBLH is less than 1 km.

Table 2 Summary statistics for comparison of HSRL-CH-derived and AQS-measured $PM_{2.5}$ for different representations of vertical mixing height. *N* is the number of data points

Height used	MAE (μg m^{-3})	NMAE	ME (μg m^{-3})	r^2	*N*
NAM PBLH	10.2	48	6.1	0.50	320
MERRA-2 PBLH	8.5	43	3.3	0.55	301
HSRL MLH	9.7	49	7.3	0.62	319

Table 3 Summary statistics when different NAM PBLH thresholds are applied to surface $PM_{2.5}$ estimates using HSRL-CH

PBLH threshold	MAE (μg m^{-3})	NMAE	ME (μg m^{-3})	r^2	*N*
No threshold	10.2	48	6.1	0.50	320
300 m	9.8	47	5.8	0.52	305
500 m	8.1	44	5.1	0.64	255
600 m	7.2	49	5.2	0.68	207
700 m	6.7	51	4.7	0.65	182

have chosen to use the NAM PBLH for detailed comparisons between HSRL-CH-derived and AQS-measured $PM_{2.5}$. This choice of NAM PBLH was made primarily to maintain consistency with the study by Meskhidze *et al.*,[20] which tested the HSRL-CH method over the Eastern US.

Building on the work of Sutherland *et al.*[22] which demonstrated improved performance of HSRL-CH estimates of surface $PM_{2.5}$ by excluding the data with HSLR-derived MLH below 600 m, we conducted a similar analysis across five measurement campaigns. Our analysis, summarized in Table 3, reveals a clear trend: as we increase the NAM PBLH threshold, we observe a reduction in MAE and an improved agreement between HSRL-CH-estimated and AQS-measured surface $PM_{2.5}$. Fig. 3 shows the dependency of MAE and r^2 on PBLH thresholds observed in this study and what was found using retrievals from the KORUS-AQ campaign and the MLH thresholds as reported by Sutherland *et al.*[22] The consistency of these results across different continents and aerosol regimes indicates that for HSRL-CH to be effectively used in monitoring $PM_{2.5}$ from spaceborne HSRL-retrievals, implementing quality control filters that remove cases of shallow mixed layers may be necessary. Alternatively, this finding points to the potential benefit of developing a hybrid approach. Such an approach would handle instances of shallow mixed layers separately, using a different methodology tailored to these challenging conditions.

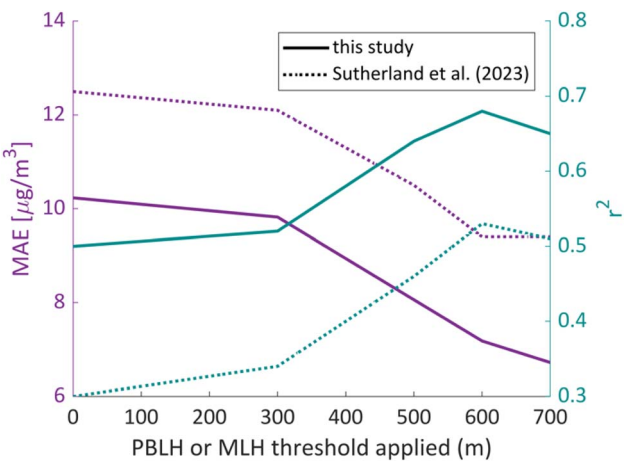

Fig. 3 Dependence of MAE (purple) and r^2 (blue) on the PBLH/MLH threshold.

4.2 $PM_{2.5}$ comparison

The five campaigns resulted in 320 instances where HSRL data were successfully retrieved within an 8 km radius of an AQS site with concurrent $PM_{2.5}$ measurements. Aggregating data from all five campaigns, we found that the HSRL-CH derived and AQS measured $PM_{2.5}$ had $r^2 = 0.5$ and MAE = 10.2 μg m^{-3} (Table 4). According to the summary statistics (Table 4), four out of the five campaigns demonstrated MAE values comparable to that found in the DISCOVER-AQ Baltimore–Washington D.C. campaign (*i.e.*, 6.2 μg m^{-3}) when using a similar methodology.[20] The outlier was the DISCOVER-AQ CA campaign (diamonds in Fig. 4), which exhibited a notably higher MAE of 14.8 μg m^{-3}. However, the DISCOVER-AQ CA campaign was also associated with generally higher aerosol loadings than those observed during the other campaigns (Fig. 4). Table 4 shows that the NMAE for DISCOVER-AQ was well within the range of that from the other campaigns.

Fig. 4 employs a sophisticated color-coding system to represent the aerosol types that dominate the boundary layer AOD for each retrieval. The coloring scheme is as follows. The outer color of each marker indicates the aerosol type that contributed the most to the AOD within the NAM PBLH (AOD_{PBLH}). In cases where multiple aerosol types significantly contribute to the AOD within the retrieval range, the inner color of the marker represents the second most dominant aerosol

Table 4 Summary statistics for results shown in Fig. 4. Subsets of the data are shown, grouped either by campaign or by the aerosol type that was assigned the majority of AOD_{PBLH}

	MAE (μg m^{-3})	NMAE	ME (μg m^{-3})	r^2	*N*
Entire dataset	10.2	48.3	6.1	0.50	320
Campaign					
DISCOVER-AQ CA	14.8	45.8	8.6	0.15	159
SEAC^{4}RS	7.2	62.2	0.5	0.06	9
DISCOVER-AQ TX	7.1	77.3	6.6	0.23	51
DISCOVER-AQ CO	4.9	50.2	2.8	0.27	89
ACEPOL	5.2	30.4	−0.3	0.64	12
Aerosol type					
Fresh smoke	10.0	25.2	−0.7	0.24	45
Smoke	23.8	63.9	19.4	0.00	40
Urban	8.1	46.3	5.1	0.57	145
Maritime	12.1	117.6	11.6	0.23	39
Dusty mix	4.6	40.3	0.3	0.51	51

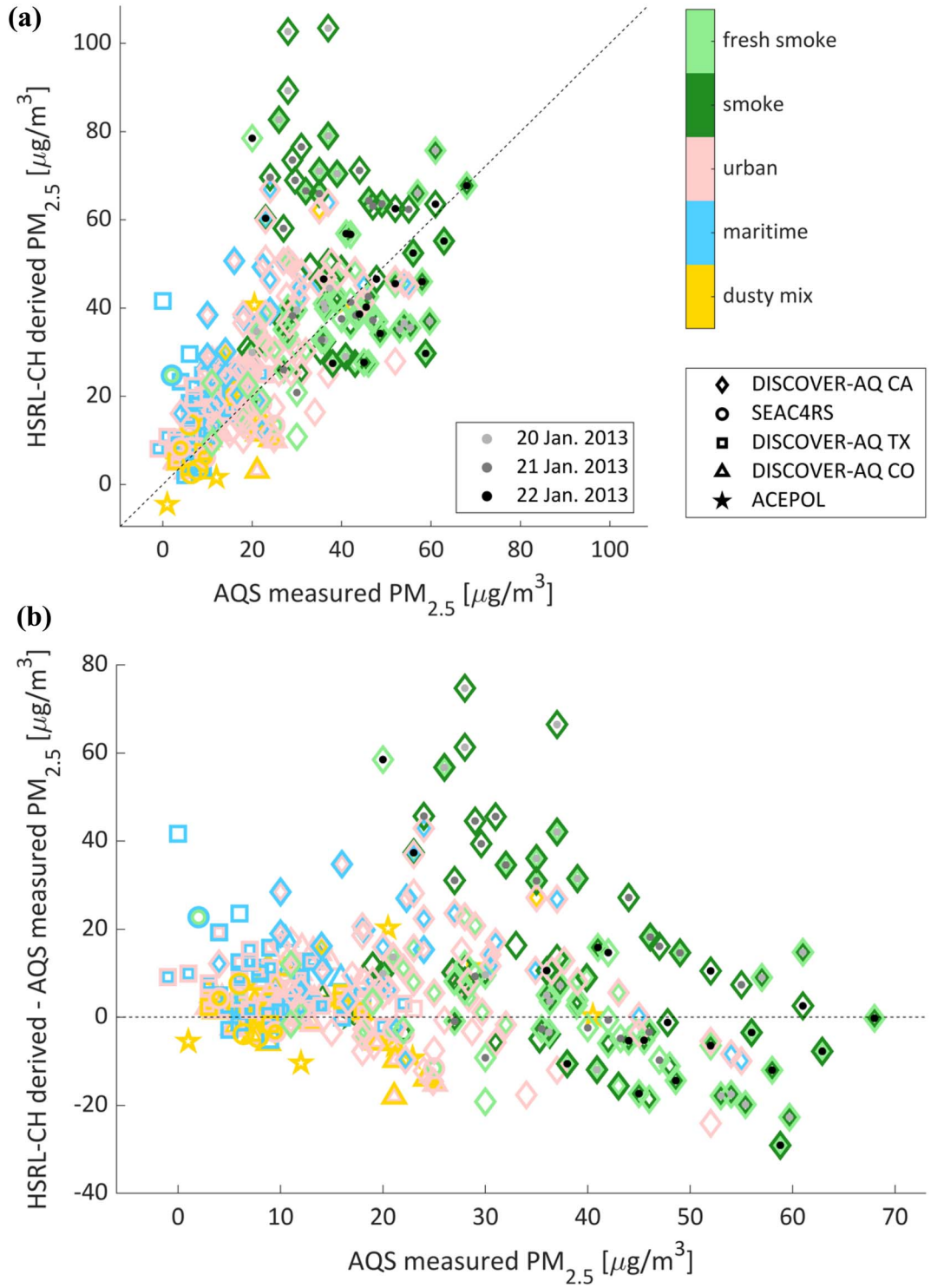

Fig. 4 (a) HSRL-CH method-derived and AQS-measured hourly $PM_{2.5}$ and (b) the difference between HSRL-CH method-derived and AQS-measured $PM_{2.5}$ as a function of AQS measurements. For each point, the outer color indicates the aerosol type that contributed the most to AOD_{PBLH}. When multiple types were derived within the same hour as the AQS measurement, the inner color shows the aerosol type that contributed the second most to AOD_{PBLH}. The shapes of the markers indicate the field campaign that the data came from. Points from 20, 21, and 22 January 2013 are indicated by light grey, grey, and black dots respectively in the center of the diamond markers.

type. This color scheme allows for the identification of general trends in aerosol composition and distribution. A notable observation from Fig. 4 is that, for this five-campaign dataset, high aerosol loadings are frequently associated with smoke and fresh smoke types. The figure provides a comprehensive visual summary of aerosol type distributions and their relative

contributions to AOD_{PBLH} across the dataset. A more detailed analysis of aerosol-type specific results is provided in Section 4.3 of the study. This section delves deeper into the chemical speciation comparison of different aerosol types and their potential impacts on $PM_{2.5}$ estimations.

4.2.1 $PM_{2.5}$ case study. The flights on 22 January 2013 provided a compelling case study, showcasing both instances of near-perfect agreement and significant discrepancies between HSRL-CH-derived and AQS-measured $PM_{2.5}$. This day's flights serve as an informative case study to explore the sources of discrepancy between derived and measured $PM_{2.5}$ and offer valuable insights into the potential sources of these discrepancies.

Fig. 5 shows a comprehensive summary of different parameters along the flight paths over the San Joaquin Valley for some of the morning flights. The full summary is given in ESI Fig. 1S.† These figures reveal a general pattern of higher $PM_{2.5}$ concentrations in the valley and lower concentrations at sites in the surrounding mountains. This distribution reflects the general circulation patterns due to its unique topography, known to contribute to the San Joaquin Valley's consistent air quality issues.[45,46] Surrounded by the Sierra Nevada Mountain Range to the east, Diablo and Santa Lucia Ranges to the west, and Tehachapi Mountains to the south, the valley experiences specific flow patterns. Air masses enter from the densely populated San Francisco Bay area to the north (also home to several refineries) and then move southward along the corridor. This unique topography often leads to air stagnation[47] and mixing with local urban, transportation, and agricultural emissions.[48–50] $PM_{2.5}$ accumulation is particularly problematic in this region during winter due to elevated combustion emissions from residential heating, lower planetary boundary layer, and weather conditions favorable for increased formation of Secondary Organic Aerosols (SOAs).[46,51]

On 22 January 2013, the flight paths intersected within an 8 km radius of six AQS sites labeled as A, B, C, K, L, and M in Fig. 5. These sites provide an excellent opportunity to explore the complexities associated with deriving $PM_{2.5}$ remotely for comparison with hourly surface measurements in complex terrains. Four of these sites are particularly noteworthy due to their diverse locations and characteristics. Sites B and M are situated within the highly populated Fresno metropolitan area, separated by 6.3 km. Their proximity and shared urban environment make them interesting points of comparison. Site L is located in the smaller city of Hanford, south of Fresno. This site represents a less urbanized area compared to the Fresno sites. Site K is positioned in the middle of a large agricultural area to the southwest of Fresno and offers a contrast to the urban locations. The varied settings of these sites – from major urban centers to smaller cities and agricultural areas – provide a range of conditions for evaluating the performance of remotely derived $PM_{2.5}$ measurements. This diversity allows for a more comprehensive assessment of the HSRL-CH methodology across different environmental contexts.

Fig. 6 illustrates the diurnal pattern of $PM_{2.5}$ concentrations, showing an initial increase between 6 and 8 am local time, likely

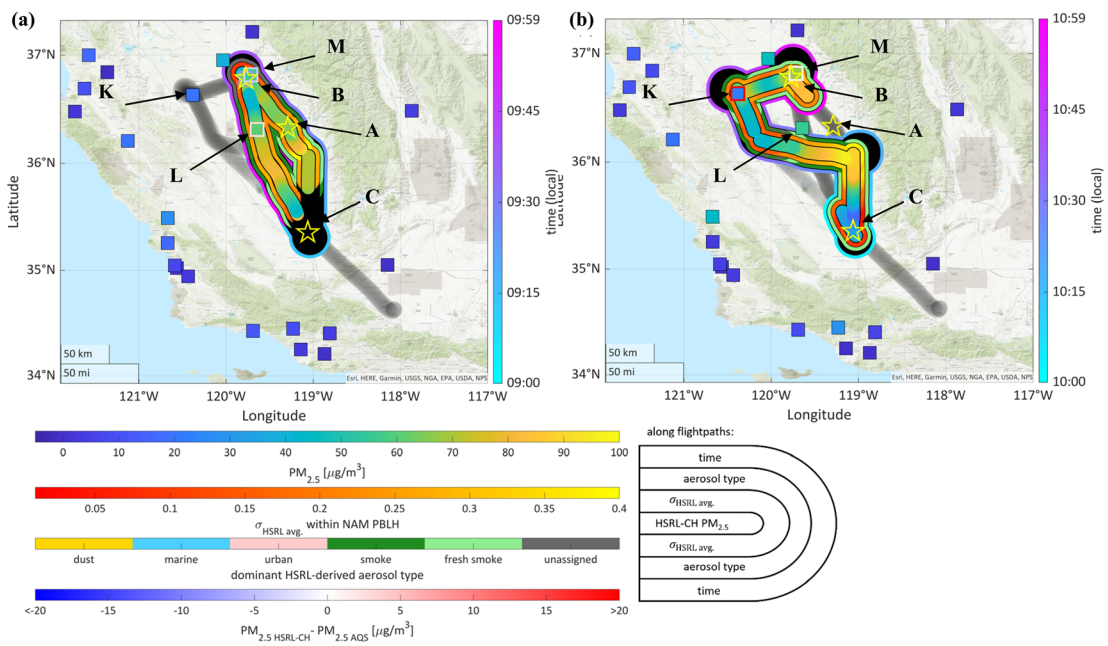

Fig. 5 (a) 09:00 and (b) 10:00 local time for the morning flight on 22 January 2013. Gray shading indicates the 8 km radius along the flight path. Along the flight path shown from the center of the flight track outward are: $PM_{2.5}$ derived using HSRL-CH, average HSRL retrieved extinction at 532 nm within the NAM PBLH, HSRL-derived aerosol type that contributed most to extinction within the NAM PBLH, and the measurement time. Square markers indicate $PM_{2.5}$ concentration measured at AQS sites for that hour. For AQS sites that are within 8 km of the flight path, the coloring of the border of the box indicates the difference between the HSRL-CH-derived $PM_{2.5}$ and the AQS measurement for that hour. Locations where daily speciation data were recorded for this day are indicated by yellow stars. Letters with arrows indicate site IDs as defined in Table 1 and ESI Table 1S.†

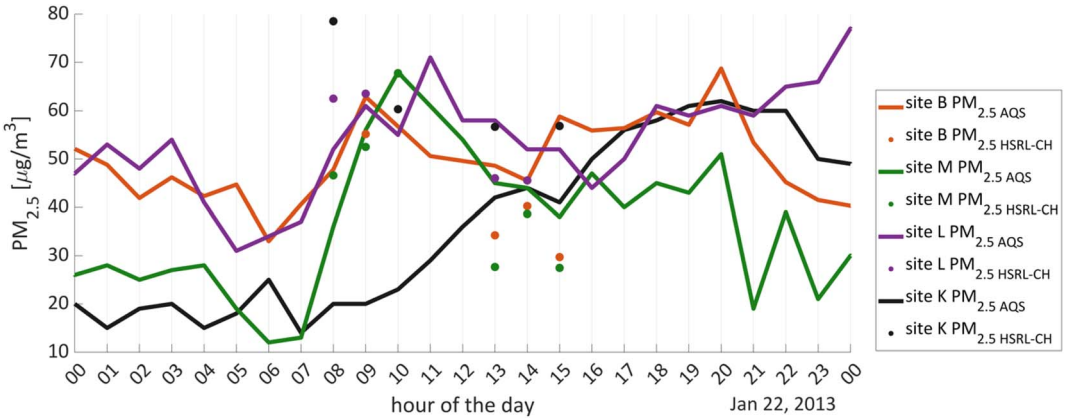

Fig. 6 Hourly $PM_{2.5}$ (local time) measured at AQS sites K, B, M, and L on 22 January 2013.

corresponding to morning rush hour traffic. In urban areas, $PM_{2.5}$ levels peak around 10 to 11 am, followed by a decrease. A secondary increase is observed later in the afternoon, presumably due to the afternoon rush hour. This $PM_{2.5}$ variability appears to be closely linked to the diurnal dynamics of the PBLH. During the day, as the PBL grows, it entrains cleaner air from above, diluting pollutants. Conversely, the afternoon reduction in PBLH and the formation of nocturnal boundary layers lead to significant near-ground pollution accumulation. An exception to this pattern is observed at site K, located in an agricultural region downwind from urban areas. Here, $PM_{2.5}$ concentrations continue to rise until later in the afternoon.

Comparing AQS-measured and HSRL-CH method-derived $PM_{2.5}$ concentrations reveals intriguing trends. For sites B, L, and M, morning concentration values show good agreement, suggesting that remotely measured extinction within the PBLH accurately represents surface conditions. Afternoon HSRL-CH-derived $PM_{2.5}$ values are notably lower than AQS measurements. This indicates that despite the general $PM_{2.5}$ reduction due to boundary layer growth, surface concentrations remain significantly higher than those inferred from the average PBLH. At site K, HSRL-CH-derived $PM_{2.5}$ values consistently exceed AQS measurements, suggesting that pollution from urban areas is advected at higher elevations without significantly impacting surface conditions. Interestingly, Fig. 6 also reveals substantial differences (up to 35 μg m^{-3}) between AQS measurements at sites B and M, despite their proximity (6.3 km apart). This discrepancy lacks a clear explanation but may be attributed to local sources influencing surface $PM_{2.5}$ values.

These results highlight the complexities involved in accurately estimating surface $PM_{2.5}$ concentrations using remote sensing techniques and underscore the importance of considering local meteorological factors and topography for diurnal variations in air quality assessments using remote sensing techniques.

4.3 Chemical speciation comparison

Our analysis will begin with an examination of the daily averages of aerosol composition across all campaigns. This approach offers a comprehensive overview of the general trends and patterns within our dataset. By focusing on these daily averages, we can establish a broad understanding of how the HSRL-CH-derived compositions compare to AQS measurements on a day-to-day basis. This initial overview helps identify overarching patterns in the data, allows us to spot potential differences between the HSRL-CH method and AQS measurements, and provides a foundation for more detailed analyses to follow. Following this broad assessment, we will transition to a more granular examination of type-specific data. This detailed analysis will explore how different aerosol types contribute to the observed compositions, investigate any type-specific variations or biases in the HSRL-CH method, and provide insights into the performance of the HSRL-CH method across various aerosol categories.

By structuring our analysis in this two-tiered approach – from general to specific – we aim to provide a comprehensive understanding of the aerosol composition data. This method allows us to capture both the broad trends across campaigns and details specific to each aerosol type. Ultimately, this analytical strategy will enable us to draw meaningful conclusions about the effectiveness and accuracy of the HSRL-CH method in characterizing aerosol compositions across diverse atmospheric conditions and geographical locations.

4.3.1 Daily averages. Fig. 7 presents a comparative analysis of daily average $PM_{2.5}$ species measurements from AQS sites against those derived using the HSRL-CH method. This comparison is inherently complex due to several factors stemming from the intricate spatiotemporal distribution of aerosols and campaign flight patterns:

(1) Temporal variability: while AQS measurements are averaged over 24 hour periods, retrievals were collected at various times throughout the day, subject to diurnal fluctuations in aerosol composition and concentration.

(2) Diversity in aerosol types: multiple aerosol types were often assigned to retrievals within an 8 km radius of the AQS sites, reflecting the heterogeneous nature of atmospheric particulate matter.

Fig. 7 displays paired data from both sources for days when AQS speciation measurements and HSRL retrievals were

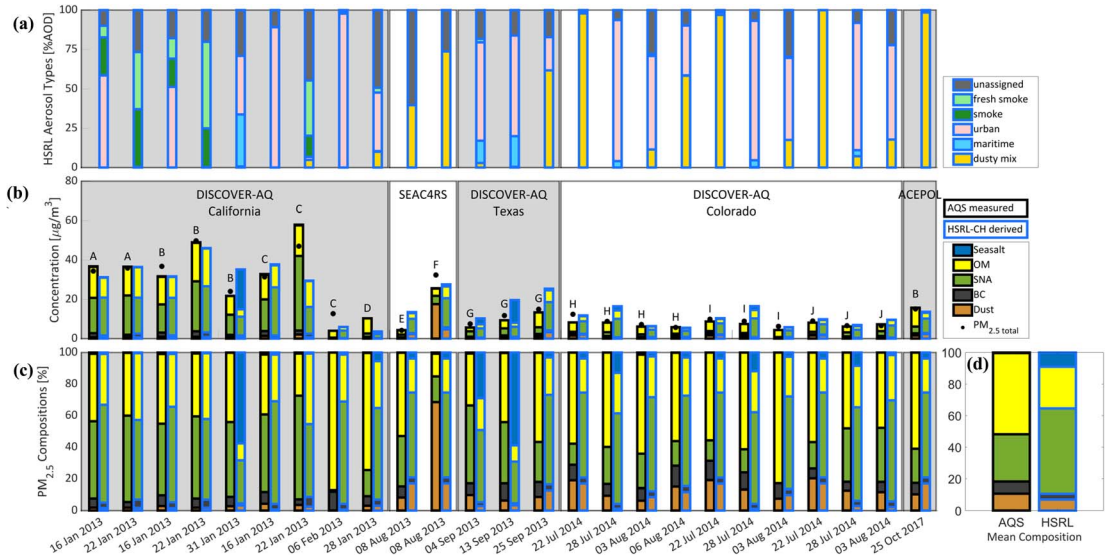

Fig. 7 Daily aerosol speciation measured at AQS sites (black outlines) and derived using HSRL-CH (blue outlines). (a) The fractional AOD_{PBLH} assigned to each aerosol type. (b) Comparison of measured and derived species concentrations. Black dots above AQS measurements indicate the total concentration as reported by the parameter code 88101 and letters above the measurements indicate the site ID (Table 1) of the AQS site. (c) Chemical speciation of $PM_{2.5}$ calculated by normalizing each species concentration from (b) by the total concentration of all species. (d) The average of all compositions from (c) for AQS and HSRL-derived compositions.

available within 8 km of the ground site. For each pair, AQS measurements appear on the left with black outlines, while HSRL retrieval-derived results appear on the right with blue outlines. Letters above the AQS data in Fig. 7(b) correspond to AQS sites listed in Table 1.

Fig. 7(a) contextualizes the HSRL-CH-derived compositions by showing the proportion of collocated AOD_{PBLH} retrievals for each aerosol type. This representation serves two purposes. First, it reveals the dominant aerosol types present during measurements, helping interpret agreements or discrepancies between HSRL-CH and AQS measurements. Second, it indicates the relative amount of HSRL-CH-derived $PM_{2.5}$ calculated using each aerosol type-specific composition shown in Fig. 1. Since AQS measurements do not classify aerosol types, only HSRL-derived results appear in this top panel.

Fig. 7(b) presents a side-by-side comparison of species concentrations from two sources: AQS-measured concentrations (black outlines) and HSRL-CH-derived concentrations (blue outlines). A critical aspect to consider when interpreting this comparison is the fundamental difference in the temporal resolution between these two datasets. HSRL-CH-derived values are based on brief periods of retrievals from random instances throughout the day when co-location conditions were met. In contrast, AQS measurements represent continuous sampling over a 24 hour period. This disparity in sampling duration and frequency is significant because numerous processes influencing surface aerosol concentration exhibit substantial diurnal variability.[52–54] Consequently, it is reasonable to anticipate considerable differences between the remotely derived, semi-instantaneous concentrations from HSRL-CH and the AQS daily observations. Understanding these inherent differences in data collection methods is crucial for accurately assessing the strengths and limitations of the HSRL-CH method in relation to traditional ground-based measurements.

Fig. 7(c) presents an alternative approach to comparing AQS-measured and HSRL-CH-derived data by examining the fractional contribution of each species to the total speciated mass, rather than absolute concentrations. This approach helps mitigate the effects of concentration variability. The analysis reveals general trends – for example, when retrievals were assigned to the maritime aerosol type, the HSRL-CH-derived composition showed a higher proportion of sea salt than that measured at the ground level. These insights into each aerosol type are explored in detail in the following section.

Fig. 7(d) offers a synthesized view, displaying the average of all fractional compositions shown in Fig. 7(c). This averaged representation reveals several notable trends in the HSRL-CH derived composition compared to AQS measurements: HSRL-CH derived composition has much higher proportions of SNA and much lower proportions of OM than those measured at the AQS sites. To a smaller degree, there is more sea salt and less BC and dust in HSRL-CH derived composition than that observed.

4.3.2 Type-specific analysis

4.3.2.1 Dusty mix aerosol type. The best agreement between HSRL-CH derived and AQS measured hourly $PM_{2.5}$ occurred when the dusty mix aerosol type contributed the most to the boundary layer AOD values. Table 4 shows that the 51 dusty mix retrievals had the lowest MAE (4.6 μg m^{-3}) and no consistent bias (ME = 0.3 μg m^{-3}). However, despite this close agreement in hourly $PM_{2.5}$, the speciation analysis (Fig. 7) reveals large differences between the AQS measured and HSRL-CH-derived chemical compositions. Fig. 7 shows that there were seven days when the dusty mix aerosol type accounted for over 50% of AOD_{PBLH}. These instances occurred at various sites and dates:

site F on 8 August 2013, site G on 25 September 2013, sites H, I, and J on 22 July 2014, site H on 6 August 2014, and site B on 25 October 2017. For these particular days, the HSRL-CH method overestimated the fraction of SNA by ~40% compared to the measured values. This overestimation of SNA was largely offset by an underestimation of OM. The fractions of other species – namely dust, sea salt, and BC – showed better agreement, with differences of about 10% or less.

The overestimation of SNA (Fig. 7(c)) in the presence of mineral dust (Fig. 7(a)) can sometimes be attributed to difficulties in aerosol type classification of complex aerosol mixtures. A notable example of this occurred on 8 August 2013, at site F, where the dusty mix aerosol type dominated AOD_{PBLH}, as shown in Fig. 7(a). On this day, AQS measurements indicated both the total concentration (Fig. 7(b)) and the fractional contribution of dust (Fig. 7(c)) to be about four times higher than those derived using the HSRL-CH method. This discrepancy can be explained by the transport of a large Saharan dust layer across the Atlantic Ocean.[55] MERRA-2 reanalysis reveals (see ESI Fig. 2S†) that $PM_{2.5}$ dust particle transport mainly occurred at the beginning of the month, with the remnants of the plume extending across Texas, Louisiana, and the Gulf of Mexico on August 8, 2013. Fig. 8 illustrates that the HSRL-assigned aerosol type within the NAM-predicted boundary layer was predominantly dusty mix along almost the entire flight path. HYSPLIT backward trajectories reveal that before reaching Marshall, Texas (site F), the air masses had traversed the Gulf of Mexico and then passed at low elevation over the highly polluted Galveston Bay/Houston area.

This trajectory offers insight into the mechanism behind the mixture of Saharan dust and anthropogenic aerosols, explaining why the particles were classified as a dusty mix rather than pure dust types. The combination of long-range transported Saharan dust with local anthropogenic pollutants resulted in a complex aerosol mixture that challenged the classification capabilities of the HSRL-CH method. It is worth noting that the high proportion of dust observed on 8 August 2013 was unique among the AQS measurements collected at site F during the campaign (see ESI Fig. 3S†).

This case study underscores the difficulties in accurately classifying and quantifying complex aerosol mixtures, particularly when long-distance transport events interact with local

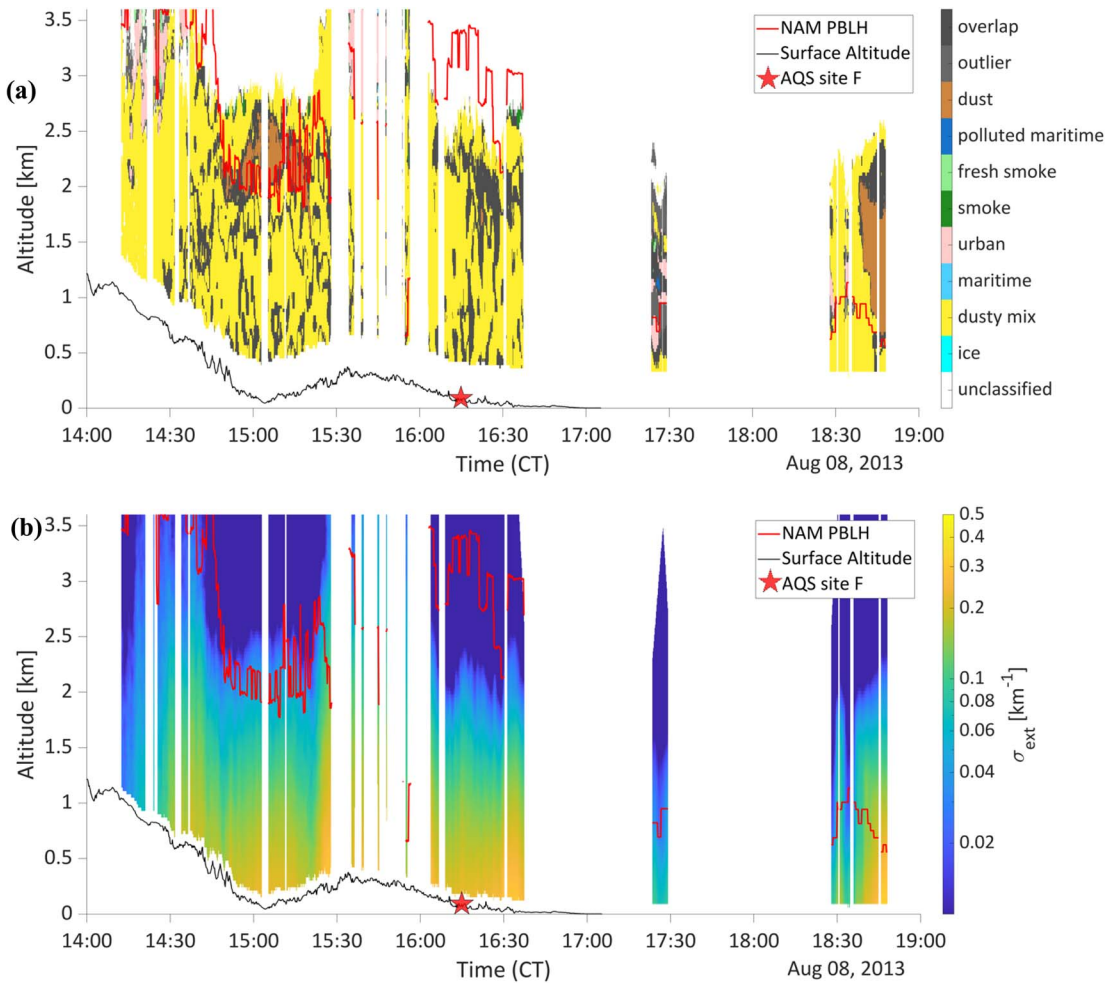

Fig. 8 (a) HSRL assigned aerosol types and (b) HSRL retrieved extinction at 532 nm along flight curtains for a portion of the 8 August 2013 flight east of the Texas/New Mexico border. The red line indicates the NAM PBLH, the thin black line indicates the surface altitude, and the stars show the location where the plane was passing within 8 km of the AQS speciation site.

pollution sources. It emphasizes two key points. The need for ongoing improvement of remote sensing techniques to refine aerosol classifications, enabling better capture of these nuanced scenarios and the importance of maintaining separate categories for pure dust and dusty mix types, rather than merging them into a single category (as was done in Fig. 1). This latter finding is consistent with research by Sutherland *et al.*,[22] which demonstrated that in South Korea, aerosol chemical composition was more accurately represented when aerosol speciation for dusty mix types was based on local measurements of aerosols in the presence of mineral dust.

4.3.2.2 Maritime aerosol type. When the maritime aerosol type contributed a discernible fraction to AOD_{PBLH}, HSRL-CH-derived hourly $PM_{2.5}$ concentrations consistently exceeded measurements from AQS sites, with MAE = 12.1 μg m^{-3} and ME = 11.6 μg m^{-3} leading to a NMAE, which was more than twice that of any other aerosol type (see Table 4). Fig. 7(a) reveals that there were no days when the majority of AOD_{PBLH} was attributed to maritime aerosol for retrievals within an 8 km radius of AQS speciation sites. The highest proportion of AOD_{PBLH} attributed to the maritime aerosol type, as shown in Fig. 7(a), was 33% observed at site B on 31 January 2013. This case will serve as a basis for examining the application of HSRL-CH in the context of maritime aerosol analysis.

HYSPLIT backward trajectories (see ESI Fig. 4S†) indicate that the air masses near site B on 31 January 2013 originated from the North Pacific and then traversed Oregon and western Nevada, passing over the Nevada Mountains before reaching Fresno, CA. On this day, two research flights were conducted over the San Joaquin Valley region. Fig. 9(a) reveals a complex vertical structure of aerosol types along the HSRL flight path. Polluted maritime aerosols were sandwiched between urban aerosols closer to the surface and dusty mix aerosols aloft. The NAM-predicted PBLH was located near the top of the polluted maritime layer. The AQS speciation data for this day (Fig. 7(c)) showed a composition of 47% SNA and 43% OM, with less than 1% sea salt. This composition supports the hypothesis that the polluted maritime aerosols were not mixed down to the surface as supported by the HSRL-retrievals. This case study highlights the importance of accurate prediction of the PBL height and the challenges in comparing remotely sensed aerosols with surface concentrations when vertical inhomogeneities exist within the predicted PBLH.

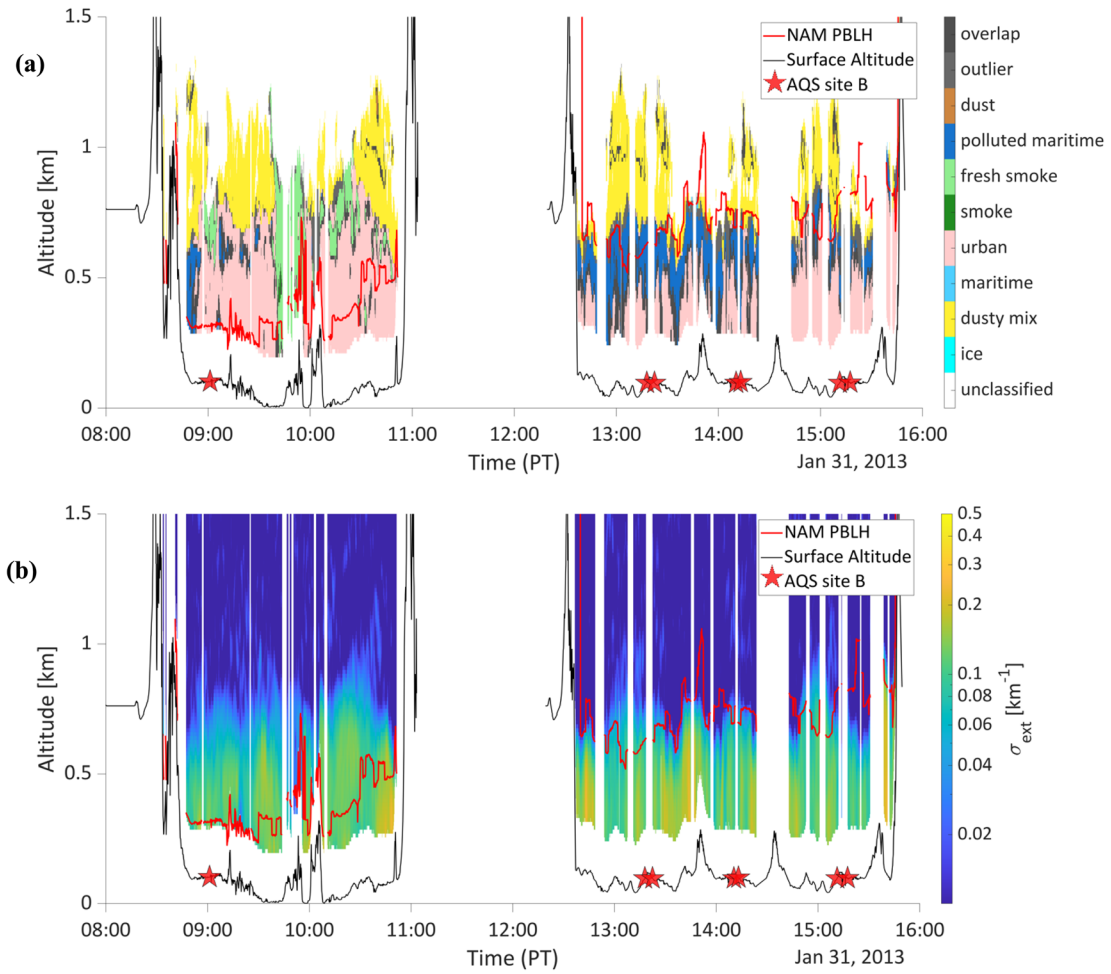

Fig. 9 (a) HSRL assigned aerosol types and (b) HSRL retrieved extinction at 532 nm along flight curtains during both morning and afternoon flights on 31 January 2013.

Fig. 9 shows that a significant fraction of aerosol extinction within the NAM-predicted PBL was attributed to the polluted maritime aerosol type. This likely explains why the HSRL-CH-derived sea salt concentration was significantly higher compared to the AQS measurements, as shown in Fig. 7(b).

For all cases with a notable presence of polluted maritime aerosols in Fig. 7(a) (*e.g.*, site B on 31 January and site G on 04 and 13 September 2013), HSRL-CH method-derived $PM_{2.5}$ concentrations were considerably higher than the AQS measurements. This is notable because sea salt is highly hygroscopic and has the highest mass extinction coefficient among aerosol species considered in this study. Because of this, an overestimate of sea salt would be expected to result in an underestimation of $PM_{2.5}$ concentration, as sea salt's ability to take up more water would yield higher extinction values and lower dry mass. However, this was not the case in our study, suggesting that the error in predicted $PM_{2.5}$ is more likely related to the non-homogeneous vertical structure of aerosols within the boundary layer.

Our analysis of the data reveals that the CATCH-derived composition for maritime aerosols, which assumes nearly 90% sea salt content (as shown in Fig. 1), may not be appropriate for use over land, particularly in urban areas. In these regions, significant amounts of anthropogenic aerosols can mix with air masses originating from the oceans, leading to a more complex aerosol composition. These findings suggest that the two types (maritime and polluted maritime) derived from HSRL measurements should be considered separately, rather than consolidated into a single category. A key improvement would be the development of a polluted maritime type within the CATCH algorithm, which would have a lower proportion of sea salt in its composition. This new category could potentially lead to better agreement between HSRL-CH-derived concentrations and measured concentrations over continental areas. By introducing this distinction, we can account for the transformation that maritime air masses undergo as they travel over land and interact with urban and industrial emissions. This approach would enhance the accuracy of the HSRL-CH method in characterizing aerosol compositions in diverse environments, particularly in coastal urban areas where marine and anthropogenic influences intersect.

4.3.2.3 Urban aerosol type. Table 4 shows that when urban aerosol types contributed the most to AOD_{PBLH}, hourly $PM_{2.5}$ had the second lowest MAE (8.1 μg m^{-3}) and the highest

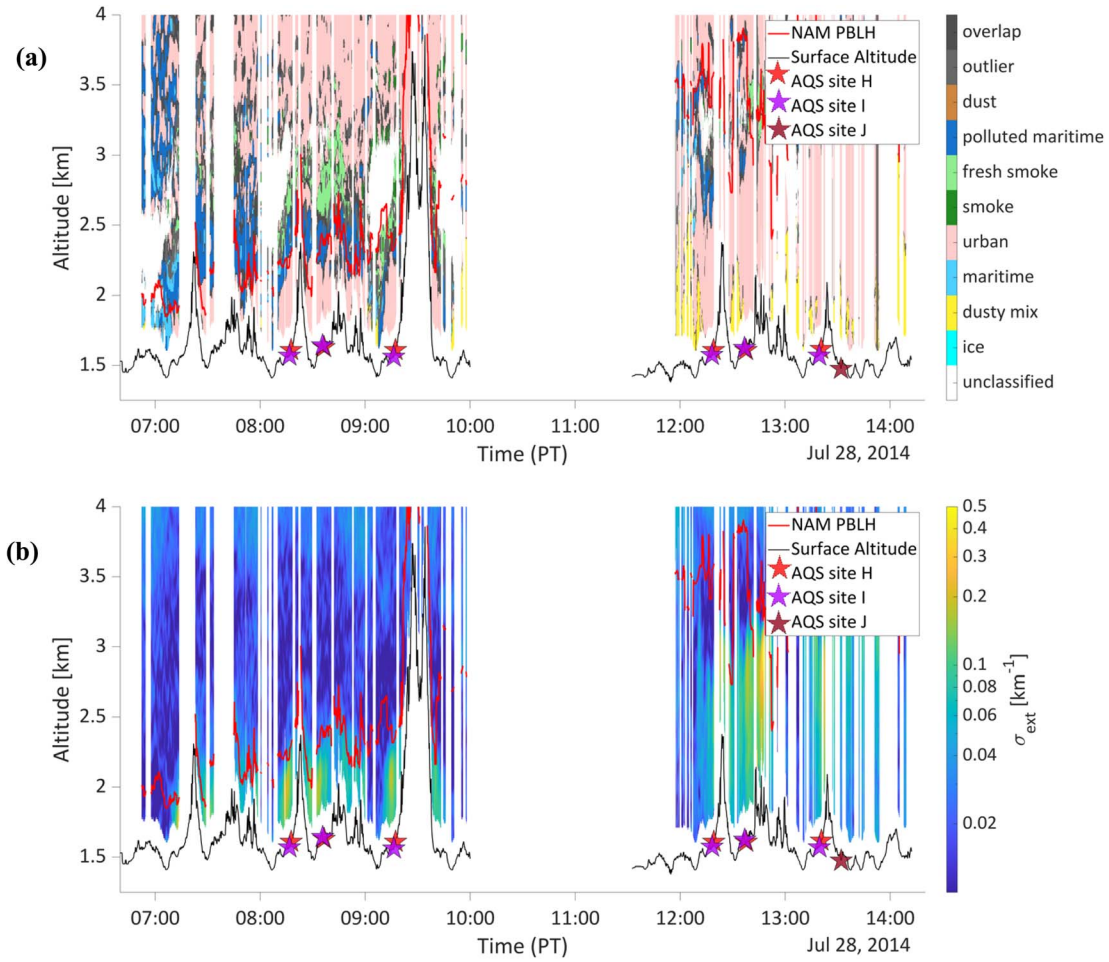

Fig. 10 (a) HSRL assigned aerosol types and (b) HSRL retrieved extinction at 532 nm along flight curtains during both morning and afternoon flights on 28 July 2014.

coefficient of determination ($r^2 = 0.57$) when comparing HSRL-CH predictions to AQS measurements. Fig. 7(a) shows 12 days when over 50% of the AOD_{PBLH} was assigned to the urban type. These instances occurred at sites A, B, and C on 16 January 2013, site C on 6 February 2013, site G on 4 September 2013 and 13 September 2013, sites H, I, and J on 28 July 2014 and 3 August 2014. For the urban aerosol type, Fig. 7(c) generally indicates that the HSRL-CH method tends to overestimate SNA concentrations while underestimating organic aerosols when compared to the AQS measurements.

On 28 July 2014, 90%, 89%, and 81% of AOD_{PBLH} near sites H, I, and J respectively were classified as urban (Fig. 7(a)). Sites H and I are located in the greater Denver metropolitan area, while site J is located in the more rural town of Platteville about 43 km to the north. Fig. 10 shows a complex mixture of aerosols in this region. During the DISCOVER-AQ Colorado campaign, all AQS-measured compositions from these sites showed 48% or more OM, yet the proportion of organics derived using HSRL-CH was 22% to 35% lower than the measured values (see Fig. 7(c)). We attribute this significant underestimation of organic aerosols to a distinct chemical signature of aerosols classified as urban by the HSRL in this region. This high proportion of organics may be linked to Colorado's oil and gas industry. By 2017, Colorado had over 53 000 active oil and natural gas wells, with a large concentration northeast of Denver.[56] Oil and gas production is known to generate enhanced levels of volatile organic compounds (VOCs),[56–58] which can lead to the formation of SOAs. Bahreini *et al.* found that in the area surrounding Denver, plumes influenced by oil and natural gas emissions had 40% higher OA concentration than plumes influenced by urban emissions.[59]

4.3.2.4 Smoke and fresh smoke aerosol types. The majority of retrievals classified as smoke or fresh smoke type occurred on 20, 21, or 22 January 2013. These data points are represented by grey-to-black dots within the diamond markers in Fig. 4. During these days, a mixture of smoke and fresh smoke aerosols was observed along the flight curtains, with many retrievals within an 8 km radius of AQS sites. Due to their comparable chemical composition (as shown in Fig. 1), we combined these two types for comparison with AQS speciation measurements.

Table 4 shows that the largest differences between the HSRL-CH-derived and AQS-measured hourly $PM_{2.5}$ concentrations occurred when the smoke aerosol type was the primary contributor to AOD_{PBLH}. For these cases, the MAE was 23.8 μg

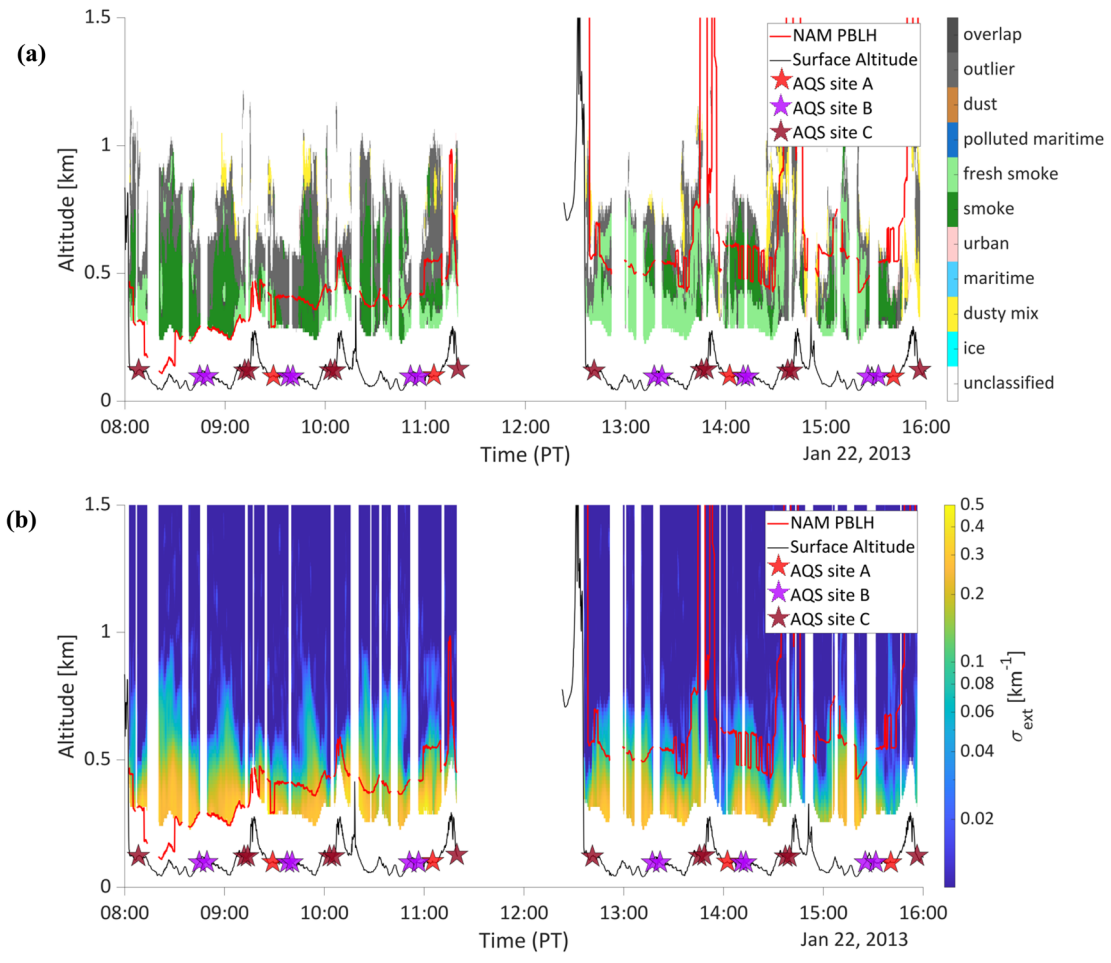

Fig. 11 (a) HSRL assigned aerosol types and (b) HSRL retrieved extinction at 532 nm along flight curtains during both morning and afternoon flights on 22 January 2013.

m^{-3} and there was no correlation between HSRL-CH-derived and AQS-measured hourly $PM_{2.5}$ ($r^2 \sim 0$, as shown in Table 4). However, cases where the fresh smoke aerosol type was the main contributor to AOD_{PBLH} generally showed much better performance. These instances had a lower MAE of 10.0 μg m^{-3}, and minimal bias, with a ME of −0.7 μg m^{-3} (as shown in Table 4). While Table 4 shows that fresh smoke aerosols were associated with the lowest NMAE, smoke aerosols were associated with the second highest, showcasing the contrast in success between these two types.

The discrepancy between measured and derived $PM_{2.5}$ concentrations during smoke events may be linked to PBLH prediction accuracy. As illustrated in Fig. 11, smoke and fresh smoke aerosols typically concentrate at altitudes between 250 and 500 m above ground level. When the planetary boundary layer expands, these elevated aerosol layers can be mixed downward, significantly influencing surface $PM_{2.5}$ concentrations recorded at AQS monitoring stations.

Although HSRL-CH-derived and AQS-measured hourly $PM_{2.5}$ concentrations generally showed poor correlation across the dataset ($n = 95$), we observed remarkably good agreement in two specific cases. These cases occurred on January 22, 2013, when smoke and fresh smoke aerosols accounted for more than 50% of AOD_{PBLH} (Fig. 7(a)) within an 8 km radius of AQS sites with available chemical composition data. According to Fig. 7(b), the difference between HSRL-CH-derived and AQS-measured total $PM_{2.5}$ concentrations was minimal: 0.2 μg m^{-3} at site A and 3.0 μg m^{-3} at site B (both less than a 5% difference). Furthermore, the chemical composition analysis (Fig. 7(c)) showed excellent agreement between both sites. In contrast, measurements at AQS site C on the same day showed weaker agreement. At this location, AQS measurements indicated notably higher SNA concentrations compared to HSRL-CH-derived values, as shown in Fig. 7(c). For comprehensive reference, ESI Fig. 5S† provides the complete dataset of retrieved extinction values and the corresponding aerosol type classifications for all flight curtains across all campaigns.

5 Conclusions

In this study, we employ HSRL retrievals of aerosol extinction and assign aerosol types to estimate surface $PM_{2.5}$ concentration and chemical composition using the HSLR-CH methodology. Previously developed and evaluated by Meskhidze *et al.*[20] and Sutherland *et al.*,[22] HSRL-CH was extensively tested using the data from five additional field campaigns: DISCOVER-AQ California, SEAC^{4}RS, DISCOVER-AQ Texas, DISCOVER-AQ Colorado, and ACEPOL. This comprehensive dataset yielded 320 datapoints for hourly $PM_{2.5}$ and 25 cases for aerosol chemical speciation comparison.

5.1. Our analysis revealed several key findings

1. Dusty mix aerosols: when this type contributed most to AOD_{PBLH}, we observed the lowest Mean Absolute Error (MAE) of 4.6 μg m^{-3} and negligible bias (Mean Error, ME = 0.3 μg m^{-3}). However, HSRL-CH derived composition typically had ∼40% more Sulfate–Nitrate–Ammonium (SNA) than the AQS-measured composition with a compensating underrepresentation of Organic Matter (OM). This discrepancy may be due to the mixing of dust with urban aerosols, as seen in the Houston metro area on August 8, 2013.

2. Maritime aerosols: retrievals dominated by this type led to consistent overestimation of $PM_{2.5}$ (ME = 11.6 μg m^{-3}) by the HSRL-CH method. The CATCH-derived maritime aerosol composition, being ∼90% sea salt, resulted in significant sea salt aerosol overestimation whenever the maritime type was assigned.

3. Urban aerosols: these showed the second lowest MAE (8.1 μg m^{-3}). However, higher urban aerosol amounts generally correlated with larger differences between AQS measured and HSRL-CH derived compositions, typically overestimating SNA and underestimating OM.

4. Smoke and fresh smoke aerosols: smoke-dominated retrievals showed the largest differences between HSRL-CH derived and AQS-measured $PM_{2.5}$, with an MAE of 23.8 μg m^{-3}. Fresh smoke aerosols performed better, with an MAE of 10.0 μg m^{-3}. Interestingly, despite these large errors, the HSRL-CH-derived composition for smoke and fresh smoke dominated days showed the best agreement with AQS-measured composition.

5. Planetary boundary layer heights (PBLHs): our study underscores the critical importance of accurately determining PBLHs in deriving surface concentrations using remotely sensed data. The vertical extent of retrievals included in these derivations significantly impacts the results. We observed that in several instances, discrepancies between AQS-measured and HSRL-CH-derived aerosol compositions could be attributed to layers of different aerosol types aloft compared to those near the surface. These aloft layers, while included in the HSRL-CH-derived composition, may not be reflected in the AQS-measured speciation, suggesting that they might not be within the atmospheric layer mixing down to the surface. Consistent with Sutherland *et al.*,[22] we found that the best results occur with high boundary layers. This is likely because when the boundary layer is low, errors in its designation have a disproportionate effect on surface concentration calculations, as these are based on a smaller number of retrievals. For example, if the PBLH is set 100 m too high this would result in the inclusion of an additional 100 m of retrievals, which may not be representative of the surface conditions. For atmospheric conditions with a high PBLH (say 1 to 1.5 km), including this additional 100 m will minimally affect results averaged across the entire layer. However, when the PBLH is low (say 500 m or below) the additional 100 m of retrievals will comprise a higher proportion of the total retrievals and significantly impact the results. In our analysis, we compared the results using three different methods to determine the vertical extent of retrievals for surface concentration derivation: NAM PBLH, MERRA2 PBLH, and HSRL MLH. We found that the choice of the vertically mixed layer led to about 20% variability in the MAE when comparing HSRL-CH-derived $PM_{2.5}$ to AQS surface measurements.

These findings have important implications for the future development of the HSRL-CH methodology:

1. Separate compositions should be developed for dust and dusty mix aerosol types for use with HSRL-CH.

2. Distinct maritime and polluted maritime aerosol type compositions should be created for HSRL-CH, as the current CATCH-derived maritime type composition is unsuitable for use over land.

3. The discrepancies in urban aerosol chemical composition estimations should be further investigated. This may be particularly important in the regions where aerosol chemical composition is strongly dominated by a particular industrial sector.

4. The reasons behind the good compositional agreement but poor concentration estimates for smoke and fresh smoke aerosols should be explored.

5. Given that one of the primary motivations for developing the HSRL-CH method is to create a model-independent approach for deriving surface $PM_{2.5}$, efforts should concentrate on determining the best way to derive the vertically mixed layer directly from the HSRL retrievals.

This approach would enhance the HSRL-CH method's independence and improve its accuracy across various atmospheric conditions and geographical locations.

Data availability

HSRL data for each campaign were obtained from the data archives DISCOVER-AQ: **https://www-air.larc.nasa.gov/missions/discover-aq/discover-aq.html**, SEAC^{4}RS: **https://www-air.larc.nasa.gov/cgi-bin/ArcView/seac4rs?DC8=1**, and ACEPOL: **https://www-air.larc.nasa.gov/cgi-bin/ArcView/acepol**. Hourly $PM_{2.5}$ data (88 101) from AQS sites were obtained for 2013, 2014, and 2017 from **https://aqs.epa.gov/aqsweb/airdata/download_files.html**. Daily speciation data were downloaded for each site from **https://www.epa.gov/outdoor-air-quality-data/interactive-map-air-quality-monitors**.

Author contributions

B. S. and N. M. conceptualized the study and carried out the investigation. B. S. wrote the software, carried out the formal analysis, and carried out the validation of the results. B. S. is in charge of the data curation. B. S. and N. M. were involved in funding acquisition. N. M. developed the initial methodology, supervised the work, and carried out project administration. B. S. wrote the original draft and N. M. carried out the review and editing.

Conflicts of interest

There are no conflicts to declare.

Acknowledgements

This research is supported by Future Investigators in NASA Earth and Space Science and Technology (FINESST) through Grant # 80NSSC22K1545. We acknowledge the computing resources provided by the North Carolina State University High Performance Computing Services Core Facility (RRID:SCR_022168).

References

1 R. Burnett, H. Chen, M. Szyszkowicz, N. Fann, B. Hubbell, C. A. Pope, J. S. Apte, M. Brauer, A. Cohen, S. Weichenthal, J. Coggins, Q. Di, B. Brunekreef, J. Frostad, S. S. Lim, H. Kan, K. D. Walker, G. D. Thurston, R. B. Hayes, C. C. Lim, M. C. Turner, M. Jerrett, D. Krewski, S. M. Gapstur, W. R. Diver, B. Ostro, D. Goldberg, D. L. Crouse, R. V. Martin, P. Peters, L. Pinault, M. Tjepkema, A. Van Donkelaar, P. J. Villeneuve, A. B. Miller, P. Yin, M. Zhou, L. Wang, N. A. H. Janssen, M. Marra, R. W. Atkinson, H. Tsang, T. Quoc Thach, J. B. Cannon, R. T. Allen, J. E. Hart, F. Laden, G. Cesaroni, F. Forastiere, G. Weinmayr, A. Jaensch, G. Nagel, H. Concin and J. V. Spadaro, Global estimates of mortality associated with long-term exposure to outdoor fine particulate matter, *Proc. Natl. Acad. Sci. U.S.A.*, 2018, **115**, 9592–9597.

2 C. J. L. Murray, A. Y. Aravkin, P. Zheng, C. Abbafati, K. M. Abbas, M. Abbasi-Kangevari, F. Abd-Allah, A. Abdelalim, M. Abdollahi, I. Abdollahpour, K. H. Abegaz, H. Abolhassani, V. Aboyans, L. G. Abreu, M. R. M. Abrigo, A. Abualhasan, L. J. Abu-Raddad, A. I. Abushouk, M. Adabi, V. Adekanmbi, A. M. Adeoye, O. O. Adetokunboh, D. Adham, S. M. Advani, G. Agarwal, S. M. K. Aghamir, A. Agrawal, T. Ahmad, K. Ahmadi, M. Ahmadi, H. Ahmadieh, M. B. Ahmed, T. Y. Akalu, R. O. Akinyemi, T. Akinyemiju, B. Akombi, C. J. Akunna, F. Alahdab, Z. Al-Aly, K. Alam, S. Alam, T. Alam, F. M. Alanezi, T. M. Alanzi, B. W. Alemu, K. F. Alhabib, M. Ali, S. Ali, G. Alicandro, C. Alinia, V. Alipour, H. Alizade, S. M. Aljunid, F. Alla, P. Allebeck, A. Almasi-Hashiani, H. M. Al-Mekhlafi, J. Alonso, K. A. Altirkawi, M. Amini-Rarani, F. Amiri, D. A. Amugsi, R. Ancuceanu, D. Anderlini, J. A. Anderson, C. L. Andrei, T. Andrei, C. Angus, M. Anjomshoa, F. Ansari, A. Ansari-Moghaddam, I. C. Antonazzo, C. A. T. Antonio, C. M. Antony, E. Antriyandarti, D. Anvari, R. Anwer, S. C. Y. Appiah, J. Arabloo, M. Arab-Zozani, F. Ariani, B. Armoon, J. Ärnlöv, A. Arzani, M. Asadi-Aliabadi, A. A. Asadi-Pooya, C. Ashbaugh, M. Assmus, Z. Atafar, D. D. Atnafu, M. M. W. Atout, F. Ausloos, M. Ausloos, B. P. Ayala Quintanilla, G. Ayano, M. A. Ayanore, S. Azari, G. Azarian, Z. N. Azene, A. Badawi, A. D. Badiye, M. A. Bahrami, M. H. Bakhshaei, A. Bakhtiari, S. M. Bakkannavar, A. Baldasseroni, K. Ball, S. H. Ballew, D. Balzi, M. Banach, S. K. Banerjee, A. B. Bante, A. G. Baraki, S. L. Barker-Collo, T. W. Bärnighausen, L. H. Barrero, C. M. Barthelemy, L. Barua, S. Basu, B. T. Baune, M. Bayati, J. S. Becker, N. Bedi, E. Beghi, Y. Béjot, M. L. Bell, F. B. Bennitt, I. M. Bensenor, K. Berhe, A. E. Berman, A. S. Bhagavathula, R. Bhageerathy, N. Bhala, D. Bhandari, K. Bhattacharyya, Z. A. Bhutta,

A. Bijani, B. Bikbov, M. S. Bin Sayeed, A. Biondi, B. M. Birihane, C. Bisignano, R. K. Biswas, H. Bitew, S. Bohlouli, M. Bohluli, A. S. Boon-Dooley, G. Borges, A. M. Borzì, S. Borzouei, C. Bosetti, S. Boufous, D. Braithwaite, N. J. K. Breitborde, S. Breitner, H. Brenner, P. S. Briant, A. N. Briko, N. I. Briko, G. B. Britton, D. Bryazka, B. R. Bumgarner, K. Burkart, R. T. Burnett, S. Burugina Nagaraja, Z. A. Butt, F. L. Caetano Dos Santos, L. E. Cahill, L. L. A. Cámera, I. R. Campos-Nonato, R. Cárdenas, G. Carreras, J. J. Carrero, F. Carvalho, J. M. Castaldelli-Maia, C. A. Castañeda-Orjuela, G. Castelpietra, F. Castro, K. Causey, C. R. Cederroth, K. M. Cercy, E. Cerin, J. S. Chandan, K.-L. Chang, F. J. Charlson, V. K. Chattu, S. Chaturvedi, N. Cherbuin, O. Chimed-Ochir, D. Y. Cho, J.-Y. J. Choi, H. Christensen, D.-T. Chu, M. T. Chung, S.-C. Chung, F. M. Cicuttini, L. G. Ciobanu, M. Cirillo, T. K. D. Classen, A. J. Cohen, K. Compton, O. R. Cooper, V. M. Costa, E. Cousin, R. G. Cowden, D. H. Cross, J. A. Cruz, S. M. A. Dahlawi, A. A. M. Damasceno, G. Damiani, L. Dandona, R. Dandona, W. J. Dangel, A.-K. Danielsson, P. I. Dargan, A. M. Darwesh, A. Daryani, J. K. Das, R. Das Gupta, J. Das Neves, C. A. Dávila-Cervantes, D. V. Davitoiu, D. De Leo, L. Degenhardt, M. DeLang, R. P. Dellavalle, F. M. Demeke, G. T. Demoz, D. G. Demsie, E. Denova-Gutiérrez, N. Dervenis, G. P. Dhungana, M. Dianatinasab, D. Dias Da Silva, D. Diaz, Z. S. Dibaji Forooshani, S. Djalalinia, H. T. Do, K. Dokova, F. Dorostkar, L. Doshmangir, T. R. Driscoll, B. B. Duncan, A. R. Duraes, A. W. Eagan, D. Edvardsson, N. El Nahas, I. El Sayed, M. El Tantawi, I. Elbarazi, I. Y. Elgendy, S. I. El-Jaafary, I. R. Elyazar, S. Emmons-Bell, H. E. Erskine, S. Eskandarieh, S. Esmaeilnejad, A. Esteghamati, K. Estep, A. Etemadi, A. E. Etisso, J. Fanzo, M. Farahmand, M. Fareed, R. Faridnia, A. Farioli, A. Faro, M. Faruque, F. Farzadfar, N. Fattahi, M. Fazlzadeh, V. L. Feigin, R. Feldman, S.-M. Fereshtehnejad, E. Fernandes, G. Ferrara, A. J. Ferrari, M. L. Ferreira, I. Filip, F. Fischer, J. L. Fisher, L. S. Flor, N. A. Foigt, M. O. Folayan, A. A. Fomenkov, L. M. Force, M. Foroutan, R. C. Franklin, M. Freitas, W. Fu, T. Fukumoto, J. M. Furtado, M. M. Gad, E. Gakidou, S. Gallus, A. L. Garcia-Basteiro, W. M. Gardner, B. S. Geberemariyam, A. A. A. A. Gebreslassie, A. Geremew, A. Gershberg Hayoon, P. W. Gething, M. Ghadimi, K. Ghadiri, F. Ghaffarifar, M. Ghafourifard, F. Ghamari, A. Ghashghaee, H. Ghiasvand, N. Ghith, A. Gholamian, R. Ghosh, P. S. Gill, T. G. G. Ginindza, G. Giussani, E. V. Gnedovskaya, S. Goharinezhad, S. V. Gopalani, G. Gorini, H. Goudarzi, A. C. Goulart, F. Greaves, M. Grivna, G. Grosso, M. I. M. Gubari, H. C. Gugnani, R. A. Guimarães, R. A. Guled, G. Guo, Y. Guo, R. Gupta, T. Gupta, B. Haddock, N. Hafezi-Nejad, A. Hafiz, A. Haj-Mirzaian, A. Haj-Mirzaian, B. J. Hall, I. Halvaei, R. R. Hamadeh, S. Hamidi, M. S. Hammer, G. J. Hankey, H. Haririan, J. M. Haro, A. I. Hasaballah, M. M. Hasan, E. Hasanpoor, A. Hashi, S. Hassanipour, H. Hassankhani, R. J. Havmoeller, S. I. Hay, K. Hayat, G. Heidari, R. Heidari-Soureshjani, H. J. Henrikson, M. E. Herbert, C. Herteliu, F. Heydarpour, T. R. Hird, H. W. Hoek, R. Holla, P. Hoogar, H. D. Hosgood, N. Hossain, M. Hosseini, M. Hosseinzadeh, M. Hostiuc, S. Hostiuc, M. Househ, M. Hsairi, V. C. Hsieh, G. Hu, K. Hu, T. M. Huda, A. Humayun, C. K. Huynh, B.-F. Hwang, V. C. Iannucci, S. E. Ibitoye, N. Ikeda, K. S. Ikuta, O. S. Ilesanmi, I. M. Ilic, M. D. Ilic, L. R. Inbaraj, H. Ippolito, U. Iqbal, S. S. N. Irvani, C. M. S. Irvine, M. M. Islam, S. M. S. Islam, H. Iso, R. Q. Ivers, C. C. D. Iwu, C. J. Iwu, I. O. Iyamu, J. Jaafari, K. H. Jacobsen, H. Jafari, M. Jafarinia, M. A. Jahani, M. Jakovljevic, F. Jalilian, S. L. James, H. Janjani, T. Javaheri, J. Javidnia, P. Jeemon, E. Jenabi, R. P. Jha, V. Jha, J. S. Ji, L. Johansson, O. John, Y. O. John-Akinola, C. O. Johnson, J. B. Jonas, F. Joukar, J. J. Jozwiak, M. Jürisson, A. Kabir, Z. Kabir, H. Kalani, R. Kalani, L. R. Kalankesh, R. Kalhor, T. Kanchan, N. Kapoor, B. Karami Matin, A. Karch, M. A. Karim, G. M. Kassa, S. V. Katikireddi, G. A. Kayode, A. Kazemi Karyani, P. N. Keiyoro, C. Keller, L. Kemmer, P. J. Kendrick, N. Khalid, M. Khammarnia, E. A. Khan, M. Khan, K. Khatab, M. M. Khater, M. N. Khatib, M. Khayamzadeh, S. Khazaei, C. Kieling, Y. J. Kim, R. W. Kimokoti, A. Kisa, S. Kisa, M. Kivimäki, L. D. Knibbs, A. K. S. Knudsen, J. M. Kocarnik, S. Kochhar, J. A. Kopec, V. A. Korshunov, P. A. Koul, A. Koyanagi, M. U. G. Kraemer, K. Krishan, K. J. Krohn, H. Kromhout, B. Kuate Defo, G. A. Kumar, V. Kumar, O. P. Kurmi, D. Kusuma, C. La Vecchia, B. Lacey, D. K. Lal, R. Lalloo, T. Lallukka, F. H. Lami, I. Landires, J. J. Lang, S. M. Langan, A. O. Larsson, S. Lasrado, P. Lauriola, J. V. Lazarus, P. H. Lee, S. W. H. Lee, K. E. LeGrand, J. Leigh, M. Leonardi, H. Lescinsky, J. Leung, M. Levi, S. Li, L.-L. Lim, S. Linn, S. Liu, S. Liu, Y. Liu, J. Lo, A. D. Lopez, J. C. F. Lopez, P. D. Lopukhov, S. Lorkowski, P. A. Lotufo, A. Lu, A. Lugo, E. R. Maddison, P. W. Mahasha, M. M. Mahdavi, M. Mahmoudi, A. Majeed, A. Maleki, S. Maleki, R. Malekzadeh, D. C. Malta, A. A. Mamun, A. L. Manda, H. Manguerra, F. Mansour-Ghanaei, B. Mansouri, M. A. Mansournia, A. M. Mantilla Herrera, J. C. Maravilla, A. Marks, R. V. Martin, S. Martini, F. R. Martins-Melo, A. Masaka, S. Z. Masoumi, M. R. Mathur, K. Matsushita, P. K. Maulik, C. McAlinden, J. J. McGrath, M. McKee, M. M. Mehndiratta, F. Mehri, K. M. Mehta, Z. A. Memish, W. Mendoza, R. G. Menezes, E. W. Mengesha, A. Mereke, S. T. Mereta, A. Meretoja, T. J. Meretoja, T. Mestrovic, B. Miazgowski, T. Miazgowski, I. M. Michalek, T. R. Miller, E. J. Mills, G. Mini, M. Miri, A. Mirica, E. M. Mirrakhimov, H. Mirzaei, M. Mirzaei, R. Mirzaei, M. Mirzaei-Alavijeh, A. T. Misganaw, P. Mithra, B. Moazen, D. K. Mohammad, Y. Mohammad, N. Mohammad Gholi Mezerji, A. Mohammadian-Hafshejani, N. Mohammadifard, R. Mohammadpourhodki, A. S. Mohammed, H. Mohammed, J. A. Mohammed, S. Mohammed, A. H. Mokdad, M. Molokhia, L. Monasta, M. D. Mooney, G. Moradi, M. Moradi, M. Moradi-Lakeh, R. Moradzadeh, P. Moraga, L. Morawska, J. Morgado-da-Costa,

S. D. Morrison, A. Mosapour, J. F. Mosser, S. Mouodi, S. M. Mousavi, A. Mousavi Khaneghah, U. O. Mueller, S. Mukhopadhyay, E. C. Mullany, K. I. Musa, S. Muthupandian, A. F. Nabhan, M. Naderi, A. J. Nagarajan, G. Nagel, M. Naghavi, B. Naghshtabrizi, M. D. Naimzada, F. Najafi, V. Nangia, J. R. Nansseu, M. Naserbakht, V. C. Nayak, I. Negoi, J. W. Ngunjiri, C. T. Nguyen, H. L. T. Nguyen, M. Nguyen, Y. T. Nigatu, R. Nikbakhsh, M. R. Nixon, C. A. Nnaji, S. Nomura, B. Norrving, J. J. Noubiap, C. Nowak, V. Nunez-Samudio, A. Oţoiu, B. Oancea, C. M. Odell, F. A. Ogbo, I.-H. Oh, E. W. Okunga, M. Oladnabi, A. T. Olagunju, B. O. Olusanya, J. O. Olusanya, M. O. Omer, K. L. Ong, O. E. Onwujekwe, H. M. Orpana, A. Ortiz, O. Osarenotor, F. B. Osei, S. M. Ostroff, N. Otstavnov, S. S. Otstavnov, S. Øverland, M. O. Owolabi, M. P A, J. R. Padubidri, R. Palladino, S. Panda-Jonas, A. Pandey, C. D. H. Parry, M. Pasovic, D. K. Pasupula, S. K. Patel, M. Pathak, S. B. Patten, G. C. Patton, H. Pazoki Toroudi, A. E. Peden, A. Pennini, V. C. F. Pepito, E. K. Peprah, D. M. Pereira, K. Pesudovs, H. Q. Pham, M. R. Phillips, C. Piccinelli, T. M. Pilz, M. A. Piradov, M. Pirsaheb, D. Plass, S. Polinder, K. R. Polkinghorne, C. D. Pond, M. J. Postma, H. Pourjafar, F. Pourmalek, A. Poznańska, S. I. Prada, V. Prakash, D. R. A. Pribadi, E. Pupillo, Z. Quazi Syed, M. Rabiee, N. Rabiee, A. Radfar, A. Rafiee, A. Raggi, M. A. Rahman, A. Rajabpour-Sanati, F. Rajati, I. Rakovac, P. Ram, K. Ramezanzadeh, C. L. Ranabhat, P. C. Rao, S. J. Rao, V. Rashedi, P. Rathi, D. L. Rawaf, S. Rawaf, L. Rawal, R. Rawassizadeh, R. Rawat, C. Razo, S. B. Redford, R. C. Reiner, M. B. Reitsma, G. Remuzzi, V. Renjith, A. M. N. Renzaho, S. Resnikoff, N. Rezaei, N. Rezaei, A. Rezapour, P.-A. Rhinehart, S. M. Riahi, D. C. Ribeiro, D. Ribeiro, J. Rickard, J. A. Rivera, N. L. S. Roberts, S. Rodríguez-Ramírez, L. Roever, L. Ronfani, R. Room, G. Roshandel, G. A. Roth, D. Rothenbacher, E. Rubagotti, G. M. Rwegerera, S. Sabour, P. S. Sachdev, B. Saddik, E. Sadeghi, M. Sadeghi, R. Saeedi, S. Saeedi Moghaddam, Y. Safari, S. Safi, S. Safiri, R. Sagar, A. Sahebkar, S. M. Sajadi, N. Salam, P. Salamati, H. Salem, M. R. R. Salem, H. Salimzadeh, O. M. Salman, J. A. Salomon, Z. Samad, H. Samadi Kafil, E. Z. Sambala, A. M. Samy, J. Sanabria, T. G. Sánchez-Pimienta, D. F. Santomauro, I. S. Santos, J. V. Santos, M. M. Santric-Milicevic, S. Y. I. Saraswathy, R. Sarmiento-Suárez, N. Sarrafzadegan, B. Sartorius, A. Sarveazad, B. Sathian, T. Sathish, D. Sattin, S. Saxena, L. E. Schaeffer, S. Schiavolin, M. P. Schlaich, M. I. Schmidt, A. E. Schutte, D. C. Schwebel, F. Schwendicke, A. M. Senbeta, S. Senthilkumaran, S. G. Sepanlou, B. Serdar, M. L. Serre, J. Shadid, O. Shafaat, S. Shahabi, A. A. Shaheen, M. A. Shaikh, A. S. Shalash, M. Shams-Beyranvand, M. Shamsizadeh, K. Sharafi, A. Sheikh, A. Sheikhtaheri, K. Shibuya, K. D. Shield, M. Shigematsu, J. I. Shin, M.-J. Shin, R. Shiri, R. Shirkoohi, K. Shuval, S. Siabani, R. Sierpinski, I. D. Sigfusdottir, R. Sigurvinsdottir, J. P. Silva, K. E. Simpson, J. A. Singh, P. Singh, E. Skiadaresi, S. T. Skou, V. Y. Skryabin, E. U. R. Smith, A. Soheili, S. Soltani, M. Soofi, R. J. D. Sorensen, J. B. Soriano, M. B. Sorrie, S. Soshnikov, I. N. Soyiri, C. N. Spencer, A. Spotin, C. T. Sreeramareddy, V. Srinivasan, J. D. Stanaway, C. Stein, D. J. Stein, C. Steiner, L. Stockfelt, M. A. Stokes, K. Straif, J. L. Stubbs, M. B. Sufiyan, H. A. R. Suleria, R. Suliankatchi Abdulkader, G. Sulo, I. Sultan, Ł. Szumowski, R. Tabarés-Seisdedos, K. M. Tabb, T. Tabuchi, A. Taherkhani, M. Tajdini, K. Takahashi, J. S. Takala, A. T. Tamiru, N. Taveira, A. Tehrani-Banihashemi, M.-H. Temsah, G. A. Tesema, Z. T. Tessema, G. D. Thurston, M. V. Titova, H. R. Tohidinik, M. Tonelli, R. Topor-Madry, F. Topouzis, A. E. Torre, M. Touvier, M. R. R. Tovani-Palone, B. X. Tran, R. Travillian, A. Tsatsakis, L. Tudor Car, S. Tyrovolas, R. Uddin, C. D. Umeokonkwo, B. Unnikrishnan, E. Upadhyay, M. Vacante, P. R. Valdez, A. Van Donkelaar, T. J. Vasankari, Y. Vasseghian, Y. Veisani, N. Venketasubramanian, F. S. Violante, V. Vlassov, S. E. Vollset, T. Vos, R. Vukovic, Y. Waheed, M. T. Wallin, Y. Wang, Y.-P. Wang, A. Watson, J. Wei, M. Y. W. Wei, R. G. Weintraub, J. Weiss, A. Werdecker, J. J. West, R. Westerman, J. L. Whisnant, H. A. Whiteford, K. E. Wiens, C. D. A. Wolfe, S. S. Wozniak, A.-M. Wu, J. Wu, S. Wulf Hanson, G. Xu, R. Xu, S. Yadgir, S. H. Yahyazadeh Jabbari, K. Yamagishi, M. Yaminfirooz, Y. Yano, S. Yaya, V. Yazdi-Feyzabadi, T. Y. Yeheyis, C. S. Yilgwan, M. T. Yilma, P. Yip, N. Yonemoto, M. Z. Younis, T. P. Younker, B. Yousefi, Z. Yousefi, T. Yousefinezhadi, A. Y. Yousuf, C. Yu, H. Yusefzadeh, T. Zahirian Moghadam, M. Zamani, M. Zamanian, H. Zandian, M. S. Zastrozhin, Y. Zhang, Z.-J. Zhang, J. T. Zhao, X.-J. G. Zhao, Y. Zhao, M. Zhou, A. Ziapour, S. R. M. Zimsen, M. Brauer, A. Afshin and S. S. Lim, Global burden of 87 risk factors in 204 countries and territories, 1990–2019: a systematic analysis for the Global Burden of Disease Study 2019, *Lancet*, 2020, **396**, 1223–1249.

3 L. Pinault, M. Tjepkema, D. L. Crouse, S. Weichenthal, A. Van Donkelaar, R. V. Martin, M. Brauer, H. Chen and R. T. Burnett, Risk estimates of mortality attributed to low concentrations of ambient fine particulate matter in the Canadian community health survey cohort, *Environ. Health*, 2016, **15**, 18.

4 C. A. Pope, J. S. Lefler, M. Ezzati, J. D. Higbee, J. D. Marshall, S.-Y. Kim, M. Bechle, K. S. Gilliat, S. E. Vernon, A. L. Robinson and R. T. Burnett, Mortality Risk and Fine Particulate Air Pollution in a Large, Representative Cohort of U.S. Adults, *Environ. Health Perspect.*, 2019, **127**, 077007.

5 T. J. Woodruff, J. D. Parker and K. C. Schoendorf, Fine Particulate Matter ($PM_{2.5}$) Air Pollution and Selected Causes of Postneonatal Infant Mortality in California, *Environ. Health Perspect.*, 2006, **114**, 786–790.

6 U.S. EPA, *Integrated Science Assessment (ISA) for Particulate Matter (Final Report, Dec 2019)*, U.S. Environmental Protection Agency, Washington, DC, 2019.

7 D. L. Goldberg, P. Gupta, K. Wang, C. Jena, Y. Zhang, Z. Lu and D. G. Streets, Using gap-filled MAIAC AOD and WRF-

Chem to estimate daily $PM_{2.5}$ concentrations at 1 km resolution in the Eastern United States, *Atmos. Environ.*, 2019, **199**, 443–452.

8 R. V. Martin, M. Brauer, A. van Donkelaar, G. Shaddick, U. Narain and S. Dey, No one knows which city has the highest concentration of fine particulate matter, *Atmos. Environ.:X*, 2019, **3**, 100040.

9 Q. He, M. Wang and S. H. L. Yim, The spatiotemporal relationship between $PM_{2.5}$ and aerosol optical depth in China: influencing factors and implications for satellite $PM_{2.5}$ estimations using MAIAC aerosol optical depth, *Atmos. Chem. Phys.*, 2021, **21**, 18375–18391.

10 S. Kondragunta, B. Veihelmann, J. R. Chatfield, M. Chin, A. S. Christopher, A. Clements, M. A. Da Silva, R. Delgado, P. Dickerson, J. D. Diner, O. Dubovik, B. Fougnie, S. Garrigues, M. D. Giles, M. Goldberg, P. Gupta, M. Hashimoto, H. B. Henderson, N. B. Holben, K. A. Huff, A. R. Kahn, J. Kim, K. E. Knowland, N. S. Koplitz, I. Laszlo, L. B. Lefer, C. R. Levy, H. Liu, Y. Liu, D. Loyola, I. A. Lyapustin, V. R. Martin, M. Mishra, R. Muva, V. Natraj, J. M. Newchurch, B. R. Pierce, J. Price, E. P. Saide, J. J. Szykman, T. Tanaka, O. Torres, A. van Donkelaar, J. Wang, J. E. Welton and H. Zhang, *Monitoring Surface PM2.5: An International Constellation Approach to Enhancing the Role of Satellite Observations*, 2022, NOAA, DOI: 10.25923/7SNZ-VN34.

11 H. J. Lee, Y. Liu, B. A. Coull, J. Schwartz and P. Koutrakis, A novel calibration approach of MODIS AOD data to predict $PM_{2.5}$ concentrations, *Atmos. Chem. Phys.*, 2011, **11**, 7991–8002.

12 S. Philip, R. V. Martin, A. van Donkelaar, J. W.-H. Lo, Y. Wang, D. Chen, L. Zhang, P. S. Kasibhatla, S. Wang, Q. Zhang, Z. Lu, D. G. Streets, S. Bittman and D. J. Macdonald, Global Chemical Composition of Ambient Fine Particulate Matter for Exposure Assessment, *Environ. Sci. Technol.*, 2014, **48**, 13060–13068.

13 C. F. Bohren and D. R. Huffman, *Absorption and Scattering of Light by Small Particles*, Wiley-VCH, Weinheim, 2004.

14 C. A. Brock, N. L. Wagner, B. E. Anderson, A. R. Attwood, A. Beyersdorf, P. Campuzano-Jost, A. G. Carlton, D. A. Day, G. S. Diskin, T. D. Gordon, J. L. Jimenez, D. A. Lack, J. Liao, M. Z. Markovic, A. M. Middlebrook, N. L. Ng, A. E. Perring, M. S. Richardson, J. P. Schwarz, R. A. Washenfelder, A. Welti, L. Xu, L. D. Ziemba and D. M. Murphy, Aerosol optical properties in the southeastern United States in summer – Part 1: Hygroscopic growth, *Atmos. Chem. Phys.*, 2016, **16**, 4987–5007.

15 M. Pitchford, W. Malm, B. Schichtel, N. Kumar, D. Lowenthal and J. Hand, Revised Algorithm for Estimating Light Extinction from IMPROVE Particle Speciation Data, *J. Air Waste Manage. Assoc.*, 2007, **57**, 1326–1336.

16 J. Seinfeld and S. Pandis, in *Atmospheric Chemistry and Physics : from Air Pollution to Climate Change*, J. Wiley, Hoboken, N.J., 2nd edn, 2006, pp. 633–657.

17 K. Suzuki and T. Takemura, Perturbations to Global Energy Budget Due to Absorbing and Scattering Aerosols, *J. Geophys. Res.:Atmos.*, 2019, **124**, 2194–2209.

18 M. A. Burgos, E. Andrews, G. Titos, L. Alados-Arboledas, U. Baltensperger, D. Day, A. Jefferson, N. Kalivitis, N. Mihalopoulos, J. Sherman, J. Sun, E. Weingartner and P. Zieger, A global view on the effect of water uptake on aerosol particle light scattering, *Sci. Data*, 2019, **6**, 157.

19 M. D. Petters and S. M. Kreidenweis, A single parameter representation of hygroscopic growth and cloud condensation nucleus activity, *Atmos. Chem. Phys.*, 2007, **7**, 1961–1971.

20 N. Meskhidze, B. Sutherland, X. Ling, K. Dawson, M. S. Johnson, B. Henderson, C. A. Hostetler and R. A. Ferrare, Improving estimates of $PM_{2.5}$ concentration and chemical composition by application of High Spectral Resolution Lidar (HSRL) and Creating Aerosol Types from chemistry (CATCH) algorithm, *Atmos. Environ.*, 2021, **250**, 118250.

21 K. W. Dawson, N. Meskhidze, S. P. Burton, M. S. Johnson, M. S. Kacenelenbogen, C. A. Hostetler and Y. Hu, Creating Aerosol Types from CHemistry (CATCH): A New Algorithm to Extend the Link Between Remote Sensing and Models, *J. Geophys. Res.:Atmos.*, 2017, **122**(12), 366–392.

22 B. Sutherland, S. Burton, C. A. Hostetler, R. A. Ferrare, J. Hair, R. J. Park, Y. J. Oak and N. Meskhidze, Application of DIAL/HSRL and CATCH algorithm-based methodologies for surface $PM_{2.5}$ concentrations during the KORUS-AQ campaign, *Atmos. Environ.*, 2023, **301**, 119719.

23 J. W. Hair, C. A. Hostetler, A. L. Cook, D. B. Harper, R. A. Ferrare, T. L. Mack, W. Welch, L. R. Izquierdo and F. E. Hovis, Airborne High Spectral Resolution Lidar for profiling aerosol optical properties, *Appl. Opt.*, 2008, **47**, 6734.

24 S. P. Burton, C. A. Hostetler, A. L. Cook, J. W. Hair, S. T. Seaman, S. Scola, D. B. Harper, J. A. Smith, M. A. Fenn, R. A. Ferrare, P. E. Saide, E. V. Chemyakin and D. Müller, Calibration of a high spectral resolution lidar using a Michelson interferometer, with data examples from ORACLES, *Appl. Opt.*, 2018, **57**, 6061.

25 E. V. Browell, Differential absorption lidar sensing of ozone, *Proc. IEEE*, 1989, **77**, 419–432.

26 S. P. Burton, R. A. Ferrare, C. A. Hostetler, J. W. Hair, R. R. Rogers, M. D. Obland, C. F. Butler, A. L. Cook, D. B. Harper and K. D. Froyd, Aerosol classification using airborne High Spectral Resolution Lidar measurements – methodology and examples, *Atmos. Meas. Tech.*, 2012, **5**, 73–98.

27 K. Julaha, V. Ždímal, A. H. Šmejkalová, K. Komínková and N. Zíková, Boundary layer and mixing layer height: Models *vs*. Ground-based measurements intercomparison, *Atmos. Res.*, 2024, 107897.

28 R. B. Stull, *An Introduction to Boundary Layer Meteorology*, Kluwer, Dordrecht, 1988.

29 R. Dang, Y. Yang, X.-M. Hu, Z. Wang and S. Zhang, A Review of Techniques for Diagnosing the Atmospheric Boundary

Layer Height (ABLH) Using Aerosol Lidar Data, *Remote Sens.*, 2019, **11**, 1590.

30 S. Odintsov, E. Miller, A. Kamardin, I. Nevzorova, A. Troitsky and M. Schröder, Investigation of the Mixing Height in the Planetary Boundary Layer by Using Sodar and Microwave Radiometer Data, *Environments*, 2021, **8**, 115.

31 Y. Xu, B. Mitchell, R. Delgado, A. Ouyed, E. Crosbie, L. Cutler, M. Fenn, R. Ferrare, J. Hair, C. Hostetler, S. Kirschler, M. Kleb, A. Nehrir, D. Painemal, C. E. Robinson, A. J. Scarino, T. Shingler, M. A. Shook, A. Sorooshian, K. L. Thornhill, C. Voigt, H. Wang, X. Zeng and P. Zuidema, Boundary Layer Structures Over the Northwest Atlantic Derived From Airborne High Spectral Resolution Lidar and Dropsonde Measurements During the ACTIVATE Campaign, *J. Geophys. Res.:Atmos.*, 2024, **129**, e2023JD039878.

32 A. Rasheeda Satheesh, M. D. Petters and N. Meskhidze, Aerosol Vertical Turbulent Mass Flux Retrievals Through Novel Remote Sensing Algorithm, *J. Geophys. Res.:Atmos.*, 2024, **129**, e2023JD040322.

33 E. Rogers, Y. Lin, K. Mitchell, W. Wu, B. Ferrier, G. Gayno, M. Pondeca, M. Pyle, V. Wong and M. Ek, NCEP North American Modeling System: Final Eta model/analysis changes and preliminary experiments using the WRF-NMM, *Proc. 21st Conference on Weather Analysis and Forecasting/17th Conference on Numerical Weather Prediction*, American Meteorological Society, Washington, DC, 2005.

34 Global Modeling and Assimilation Office (GMAO), *MERRA-2 tavg1_2d_flx_Nx: 2d,1-Hourly,Time-Averaged, Single-Level, Assimilation, Surface Flux Diagnostics V5.12.4*, Goddard Earth Sciences Data and Information Services Center (GES DISC), Greenbelt, MD, USA, 2015, DOI: **10.5067/7MCPBJ41Y0K6**, Accessed: 10/25/2023.

35 I. M. Brooks, Finding Boundary Layer Top: Application of a Wavelet Covariance Transform to Lidar Backscatter Profiles, *J. Atmos. Ocean. Technol.*, 2003, **20**, 1092–1105.

36 A. J. Scarino, M. D. Obland, J. D. Fast, S. P. Burton, R. A. Ferrare, C. A. Hostetler, L. K. Berg, B. Lefer, C. Haman, J. W. Hair, R. R. Rogers, C. Butler, A. L. Cook and D. B. Harper, Comparison of mixed layer heights from airborne high spectral resolution lidar, ground-based measurements, and the WRF-Chem model during CalNex and CARES, *Atmos. Chem. Phys.*, 2014, **14**, 5547–5560.

37 C. M. Carrico, P. Kus, M. J. Rood, P. K. Quinn and T. S. Bates, Mixtures of pollution, dust, sea salt, and volcanic aerosol during ACE-Asia: Radiative properties as a function of relative humidity, *J. Geophys. Res.:Atmos.*, 2003, **108**, DOI: **10.1029/2003JD003405**.

38 H. J. Shin, S.-M. Park, J. S. Park, I. H. Song and Y. D. Hong, Chemical Characteristics of High PM Episodes Occurring in Spring 2014, Seoul, Korea, *Adv. Meteorol.*, 2016, **2016**, 1–11.

39 F. S. Binkowski and S. J. Roselle, Models-3 Community Multiscale Air Quality (CMAQ) model aerosol component 1. Model description, *J. Geophys. Res.*, 2003, **108**, 2001JD001409.

40 W. C. Malm and J. L. Hand, An examination of the physical and optical properties of aerosols collected in the IMPROVE program, *Atmos. Environ.*, 2007, **41**, 3407–3427.

41 R. R. Rogers, J. W. Hair, C. A. Hostetler, R. A. Ferrare, M. D. Obland, A. L. Cook, D. B. Harper, S. P. Burton, Y. Shinozuka, C. S. McNaughton, A. D. Clarke, J. Redemann, P. B. Russell, J. M. Livingston and L. I. Kleinman, NASA LaRC airborne high spectral resolution lidar aerosol measurements during MILAGRO: observations and validation, *Atmos. Chem. Phys.*, 2009, **16**, 4811–4826.

42 S. Crumeyrolle, G. Chen, L. Ziemba, A. Beyersdorf, L. Thornhill, E. Winstead, R. H. Moore, M. A. Shook, C. Hudgins and B. E. Anderson, Factors that influence surface $PM_{2.5}$ values inferred from satellite observations: perspective gained for the US Baltimore–Washington metropolitan area during DISCOVER-AQ, *Atmos. Chem. Phys.*, 2014, **14**, 2139–2153.

43 T. D. Toth, J. Zhang, M. A. Vaughan, J. S. Reid and J. R. Campbell, Retrieving particulate matter concentrations over the contiguous United States using CALIOP observations, *Atmos. Environ.*, 2022, **274**, 118979.

44 T. D. Toth, J. Zhang, J. R. Campbell, E. J. Hyer, J. S. Reid, Y. Shi and D. L. Westphal, Impact of data quality and surface-to-column representativeness on the $PM_{2.5}$/satellite AOD relationship for the contiguous United States, *Atmos. Chem. Phys.*, 2014, **14**, 6049–6062.

45 Y.-Y. Meng, R. P. Rull, M. Wilhelm, C. Lombardi, J. Balmes and B. Ritz, Outdoor air pollution and uncontrolled asthma in the San Joaquin Valley, California, *J. Epidemiol. Community Health*, 2010, **64**, 142–147.

46 D. Orozco, A. J. Beyersdorf, L. D. Ziemba, T. Berkoff, Q. Zhang, R. Delgado, C. J. Hennigan, K. L. Thornhill, D. E. Young, C. Parworth, H. Kim and R. M. Hoff, Hygrosopicity measurements of aerosol particles in the San Joaquin Valley, CA, Baltimore, MD, and Golden, CO, *J. Geophys. Res.:Atmos.*, 2016, **121**, 7344–7359.

47 D. J. Caputi, I. Faloona, J. Trousdell, J. Smoot, N. Falk and S. Conley, Residual layer ozone, mixing, and the nocturnal jet in California's San Joaquin Valley, *Atmos. Chem. Phys.*, 2019, **19**, 4721–4740.

48 X. Ge, A. Setyan, Y. Sun and Q. Zhang, Primary and secondary organic aerosols in Fresno, California during wintertime: Results from high resolution aerosol mass spectrometry, *J. Geophys. Res.:Atmos.*, 2012, **117**, DOI: **10.1029/2012JD018026**.

49 A. Sorooshian, S. M. Murphy, S. Hersey, H. Gates, L. T. Padro, A. Nenes, F. J. Brechtel, H. Jonsson, R. C. Flagan and J. H. Seinfeld, Comprehensive airborne characterization of aerosol from a major bovine source, *Atmos. Chem. Phys.*, 2008, **8**, 5489–5520.

50 J. G. Watson, J. C. Chow, J. L. Bowen, D. H. Lowenthal, S. Hering, P. Ouchida and W. Oslund, Air Quality Measurements from the Fresno Supersite, *J. Air Waste Manage. Assoc.*, 2000, **50**, 1321–1334.

51 C. D. Cappa and Q. Zhang, Characterization of $PM_{2.5}$ Episodes in the San Joaquin Valley Based on Data

Collected During the NASA DISCOVER-AQ Study in the Winter of 2013, *Report to the California Air Resources Board Research Division Project*, 2018, pp. 14–307.

52 L. Ahlm, E. D. Nilsson, R. Krejci and E. M. Ma, A comparison of dry and wet season aerosol number fluxes over the Amazon rain forest, *Atmos. Chem. Phys.*, 2010, **10**, 3063–3079.

53 J. S. Reid, R. E. Kuehn, R. E. Holz, E. W. Eloranta, K. C. Kaku, S. Kuang, M. J. Newchurch, A. M. Thompson, C. R. Trepte, J. Zhang, S. A. Atwood, J. L. Hand, B. N. Holben, P. Minnis and D. J. Posselt, Ground-based High Spectral Resolution Lidar observation of aerosol vertical distribution in the summertime Southeast United States, *J. Geophys. Res.:Atmos.*, 2017, **122**, 2970–3004.

54 J. P. Sherman and A. McComiskey, Measurement-based climatology of aerosol direct radiative effect, its sensitivities, and uncertainties from a background southeast US site, *Atmos. Chem. Phys.*, 2018, **18**, 4131–4152.

55 O. B. Toon, H. Maring, J. Dibb, R. Ferrare, D. J. Jacob, E. J. Jensen, Z. J. Luo, G. G. Mace, L. L. Pan, L. Pfister, K. H. Rosenlof, J. Redemann, J. S. Reid, H. B. Singh, A. M. Thompson, R. Yokelson, P. Minnis, G. Chen, K. W. Jucks and A. Pszenny, Planning, implementation, and scientific goals of the Studies of Emissions and Atmospheric Composition, Clouds and Climate Coupling by Regional Surveys (SEAC ^{4} RS) field mission, *J. Geophys. Res.:Atmos.*, 2016, **121**, 4967–5009.

56 D. Helmig, Air quality impacts from oil and natural gas development in Colorado, *Elem. Sci. Anth.*, 2020, **8**, 4.

57 Y. He, B. Zhao, S. Wang, R. Valorso, X. Chang, D. Yin, B. Feng, M. Camredon, B. Aumont, A. Dearden, S. H. Jathar, M. Shrivastava, Z. Jiang, C. D. Cappa, L. D. Yee, J. H. Seinfeld, J. Hao and N. M. Donahue, Formation of secondary organic aerosol from wildfire emissions enhanced by long-time ageing, *Nat. Geosci.*, 2024, **17**, 124–129.

58 A. Ragothaman and W. Anderson, Air Quality Impacts of Petroleum Refining and Petrochemical Industries, *Environments*, 2017, **4**, 66.

59 R. Bahreini, R. Ahmadov, S. A. McKeen, K. T. Vu, J. H. Dingle, E. C. Apel, D. R. Blake, N. Blake, T. L. Campos, C. Cantrell, F. Flocke, A. Fried, J. B. Gilman, A. J. Hills, R. S. Hornbrook, G. Huey, L. Kaser, B. M. Lerner, R. L. Mauldin, S. Meinardi, D. D. Montzka, D. Richter, J. R. Schroeder, M. Stell, D. Tanner, J. Walega, P. Weibring and A. Weinheimer, Sources and characteristics of summertime organic aerosol in the Colorado Front Range: perspective from measurements and WRF-Chem modeling, *Atmos. Chem. Phys.*, 2018, **18**, 8293–8312.